A FINITE ELEMENT MODEL OF FLUID FLOW IN JOINTED ROCK

BY

MARK A. JAMES

B.S., Kansas State University, 1986

A THESIS

submitted in partial fulfillment of the

requirements for the degree

MASTER OF SCIENCE

Department of Mechanical Engineering

KANSAS STATE UNIVERSITY
Manhattan, Kansas

1988

Approved by:

Daniel Swanson

Major Professor

Acknowledgments

Daniel Swenson, my advisor, deserves more than my thanks for his patience and for his moral and technical support. He taught me much more than finite elements and computer programming.

Shun Lung Su developed the fluid model which was implemented in DRACULA.

Thanks should go to Don Brown for working to get the financial support to finish this work and for helping me understand, at least to some degree, what I am modelling.

My parents always support me in everything I do. Thank you.

Table of Contents

List of Figures

List of Tables

Chapter I

Introduction

In the early 1970's the United States experienced its first energy crisis. At that time about 97% of the world's energy needs were being supplied by fossil fuels. The need for the United States to become less dependent on petroleum sources led to an extensive search for alternate energy sources. One of these alternatives is geothermal energy.

Geothermal energy is the natural heat produced within the Earth's crust by slowly decaying, naturally occurring, radioactive isotopes (i.e. uranium, thorium and potassium) and by conduction from the hotter interior regions. This energy is stored in several forms: hydrothermal reservoirs (naturally-occurring pockets of steam or hot water), geopressured reservoirs, magma reservoirs and hot dry rock reservoirs. This thesis presents a computer model suitable for analyzing hot dry rock reservoirs in two dimensions using the finite element method.

1.1 The HDR Concept

In a geothermal energy context, hot dry rock (HDR) is defined as naturally heated, unmelted crustal rock, that does not produce natural steam or hot water at commercially useful rates. HDR exists everywhere beneath the earth's surface; however, the quality of the resource depends on the local temperature gradient. At a given location, the temperatures at economical depths may not be high enough for electric power generation, but would almost everywhere be suitable for direct use in agriculture or

food and chemical processing, or for supplemental energy generation or space heating (Armstead, 1978).

The energy is extracted from a region of hot rock by circulating pressurized water in a closed loop through a man-made fracture system created by hydraulically fracturing the rock between two well-bores. The useful heat is recovered at the surface through heat exchangers; the cooled water is reinjected to recirculate through the underground loop (see Figure 1.1). Current estimates show that at depths <10 km, the HDR reservoir base contains ~32 million Quads of energy.[1] Two percent of this energy would supply the United States' nontransportation needs for about 2000 years at present consumption rates (Los Alamos annual report, 1979).

1.2 The HDR Program

The HDR program originated at Los Alamos National Laboratory (LANL) in 1970 as a feasibility study of underground heat extraction from low permeability rock. The work at LANL continued, and in 1977 the world's first HDR geothermal energy system (Phase I) was completed at Fenton Hill, New Mexico. In 1979 the system was enlarged using hydraulic fracturing and a series of additional flow tests were run. The tests led to a reasonably well defined model for the system (Los Alamos annual report, 1981). During flow tests in 1980 and 1981 heat extraction for the Phase I system rose to ~5 MW_t and the rate of water loss decreased to about 1.5% of the flow rate. An electric generator was operated at its full rated capacity of

[1] 1 Quad = 1 quadrillion (10^{15}) Btu = 334 MW centuries ~10^{18} J.

60 kwA and exceeded its overall design efficiency of 5.7%.

During 1979 a larger, deeper, hotter Phase II system was begun. The initial drilling for the two Phase II wells was in 1980. Initial hydrofracturing from the injection well in 1983 produced a fracture system quite different than observed in the Phase I wells. Figure 1.2 shows the anticipated Phase II fracture system based on an analysis of the Phase I and other HDR systems. Two types of joints make up the reservoir flow paths: vertical shear joints that are initially closed and require high pressures to open, and inclined tensile joints that are also initially closed, but require lower pressures to open. The actual Phase II fractured system determined from the location of microseismic events is three dimensional rather than planar, inclined rather than vertical, and did not hydraulically connect the two wells. Rather than continue with more hydrofracturing, the injection well was directionally redrilled in 1985 to intercept the fracture system created from the production well. This redrilling was successful, and subsequent hydrofracturing improved hydraulic communication between the two wells (Franke, 1988).

In May and June 1986 the Initial Closed loop Flow Test (ICFT) was run on the Phase II system to obtain operating characteristics needed to plan the year long Long Term Flow Test (LTFT). The LTFT will be used to predict thermal draw-down as well as other long term effects required for thorough reservoir evaluation. The 30 day ICFT succeeded with final production of about 10 MW_t at 192° C, while injecting 285 gpm at 4600 psi. The final water loss rate and flow impedance were high, 27% and 18

psi/gpm respectively, but were still declining (Kelkar et al., 1987). Birdsell and Robinson (1988) have had moderate success modeling the reservoir as an equivalent porous medium. They used the code FEHM developed by Zyvolosky et al. (1988) which includes heat and mass transport effects but currently does not include any deformable rock effects. FEHM also has the capability to perform uncoupled tracer calculations.

One of the primary goals of the HDR program has been to characterize the fractured reservoirs to allow economic analysis and prediction of reservoir production, and ultimately to determine the economic feasibility of a commercial HDR energy production site. Characterization of an HDR reservoir usually proceeds by analyzing seismic, temperature, flow rate, and tracer data. Many new diagnostic methods have been developed from the HDR programs in the U.S. and other countries including statistical microseismic event analysis, porous flow models, tracer analysis, as well as steady state and transient discrete crack flow models. This thesis presents a method for analyzing transient fluid flow in discrete cracks with coupling between the fluid flow and rock deformations. In this model, both the crack porosity and flow conductance are nonlinear functions of the fluid pressure.

1.3 Previous work

The traditional approach to modeling fluid flow through discrete fractures has been to assume viscous, incompressible flow between smooth parallel plates (Snow, 1965). This has come to be known as the "cubic law," in which the volumetric flow rate is proportional to the pressure gradient

and the joint aperture cubed (see Figure 1.3). Witherspoon et al. (1980) and Ryan (1987) verified the validity of the "cubic law" in laboratory work for laminar flow between parallel planar plates. The cubic law was verified for open joints and for closed joints down to a minimum of 4 μm. Witherspoon et al. (1980) also discussed deviations from the parallel plate model and recommends using a factor of roughness in the flow equation, particularly for high (> 10 MPa) crack closure stresses. Values for the factor of roughness vary from 1.04 to 1.78. Brown (1987) also recommends this. Su (1988) developed a finite element model for 1-D fluid flow based on the cubic law and included an uncoupled tracer model.

Several finite element models of coupled fluid flow in fractured rock masses have been developed recently. Noorishad et al. (1982) developed a code to solve two-dimensional quasi-static saturated porous media. Their results show that significant differences in pressure distribution and flow rate occur due to coupling fluid flow with rock deformations compared with the uncoupled flow solution. Hilber and Taylor (1976) developed a dynamic code for discrete fractures that takes into account the inertial effects of both the fluid and fracture movements. The code has been used to study seismic events along predetermined faults due to fluid injection. Cundall (1982) developed the Fluid Rock Interaction Program (FRIP) to analyze the dynamic behavior of discrete flow paths and discrete blocks. The blocks interact with each other as well as with the fluid. FRIP has been used for several transient response studies of a geothermal reservoir (Pine and Batchelor, 1984), (Pine and Ledingham, 1984), (Pine and Cundall, 1985).

Asgian (1988 a) also developed a discrete flow model. The FFFLOW model solves for quasi-static rock deformations and transient fluid flow in two dimensions. The continuum rock masses are linear elastic; the joints are nonlinear elastic and include both normal and shear rock stresses as well as fluid pressures. The results indicate that the enhanced permeability zone is not the same as the pressurized zone. Asgian (1988 b) studied the transient response due to different pumping rates. The studies indicate that the peak response (peak pressure, slippage, and aperture change) is less intense for lower pumping rates than for higher pumping rates of equal volumes of fluid.

1.4 Objectives and Scope

The primary objective of this thesis is to develop a finite element model of fluid flow through fractured rock. The finite element method was chosen because the governing equations for both the rock masses and fluid flow are well understood, and implementation is straight forward. The model developed is capable of solving the highly nonlinear equations and is capable of solving very large problems. Extensive use of the interactive pre- and post-processing developed by Swenson (1985) makes this model a finite element "analysis system." This thesis extends Su's (1988) work to include the coupled fluid flow - rock deformation model. This model is the second step in developing a coupled fluid flow - rock deformation - heat transfer model capable of modeling HDR reservoirs in two dimensions.

The HDR reservoir is modeled as a horizontal plane with discrete flow paths to model the fluid flow. The jointed rock mass forming the flow

paths are not porous media. Initially open joints can be modeled as empty fluid elements that fill up with time. Because of the robust solution algorithm, free floating rock masses can effectively be modeled.

In this model, as in the model developed by Su (1988) the fluid density and viscosity are assumed constant. In the next model, which will include heat transfer in both the structure as well as the fluid, the temperature dependent properties of the fluid will be handled more generally.

The remainder of the thesis is divided into 6 chapters. Chapter II presents the finite element derivations for the rock and fluid models, and Chapter III explains how these two independent models are coupled. Chapter IV describes the problems used to verify the model, and Chapter V explains results of problems that model the HDR reservoir at Fenton Hill, New Mexico. Chapter VI gives a summary of the thesis and conclusions about the results presented.

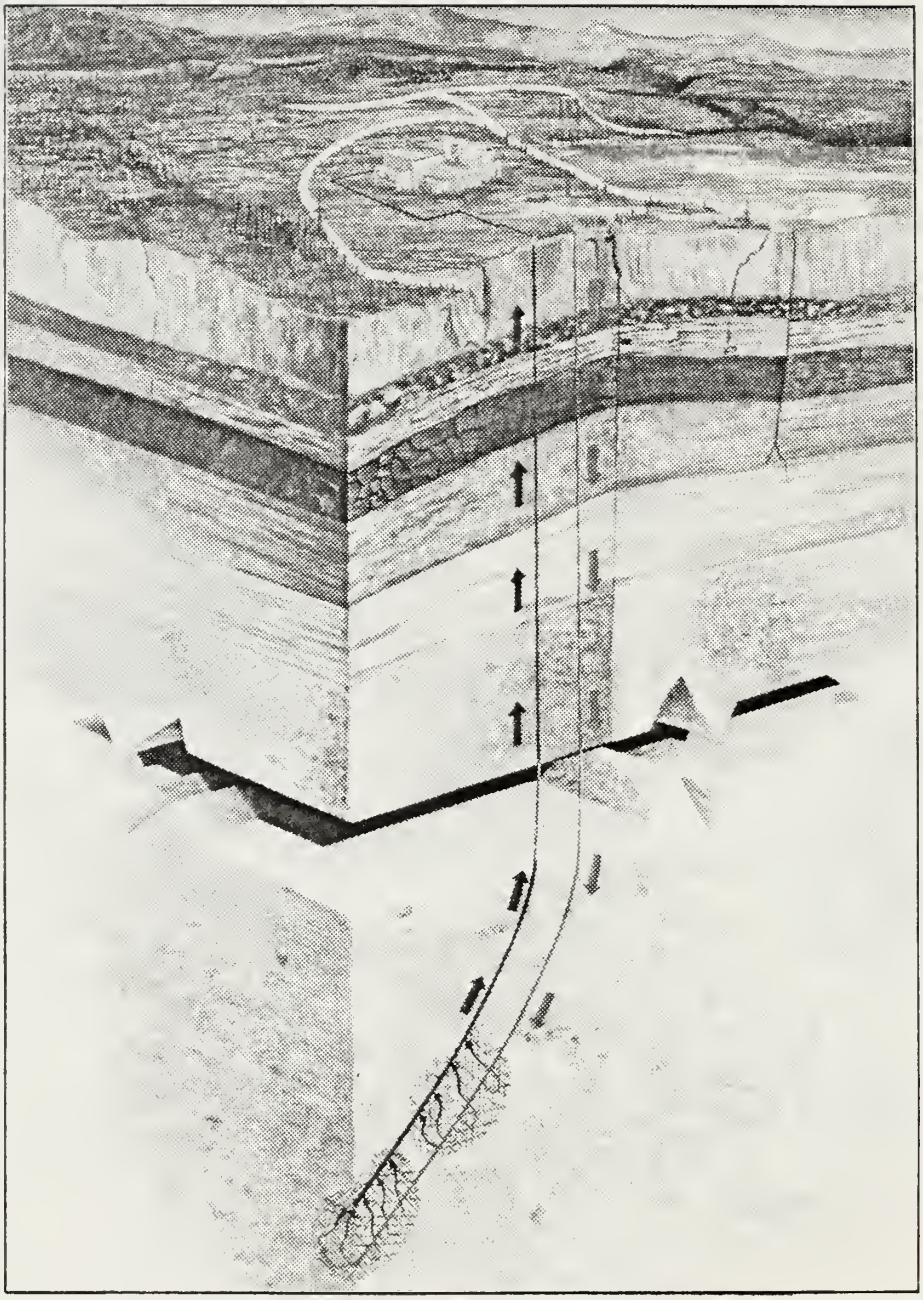

Figure 1.1: Hot Dry Rock Concept
(From LANL FY83 Report)

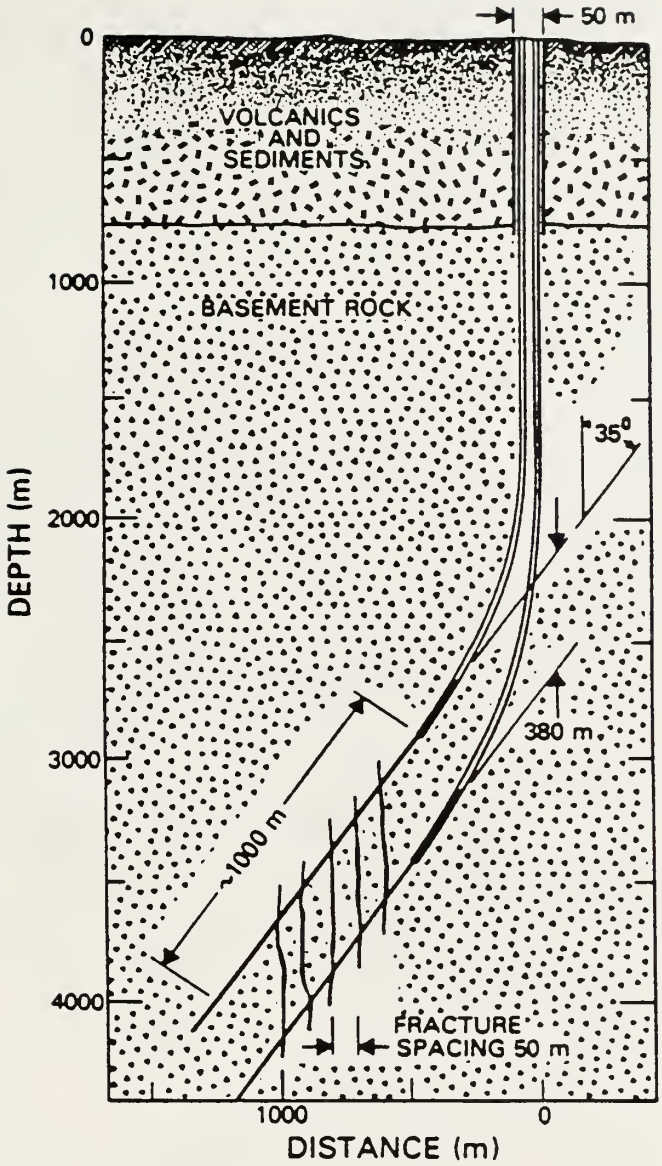

Figure 1.2: Anticipated Phase II Fracture System (From LANL FY83 Report)

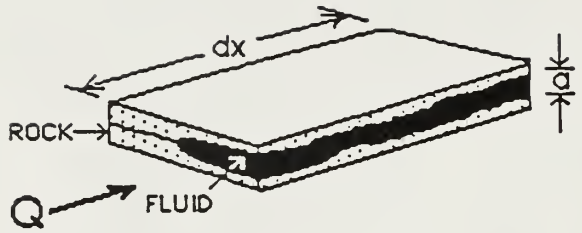

$$Q = \frac{a^3}{12\,\mu}\frac{dp}{dx}$$

Q = volumetric flow rate
a = effective joint aperture
μ = dynamic viscosity
$\frac{dp}{dx}$ = pressure gradient

FLOW RATE PROPORTIONAL TO
APPARENT JOINT APERTURE CUBED

Figure 1.3: Cubic Flow Law
(From Asgian, 1988a)

Chapter II

Finite Element Model

A finite element model of a problem gives a piecewise approximation to the governing equations. The region in which the solution is desired is divided into discrete elements and an approximate solution is assumed over the discrete element region. The contribution of each element is then added to a global system matrix, which can be solved for the nodal unknowns. The first section of this chapter develops the finite element method (FEM) for each of the four element types used in this thesis.

A joint model must have certain characteristics to model the complex relationship between the fluid flow and the joint opening. The second part of this chapter discusses some rock mechanics fundamentals and presents the joint model implementation.

In this application of FEM we are interested in solving for a set of nodal unknowns (displacements and pressures) that interact with each other through a highly nonlinear relationship. The joint displacements are a function of joint fluid pressures and a cubic function of the joint closure law, and joint flow rates are a linear function of joint pressure gradients and a cubic function of joint displacements. The third part of this chapter describes the solution method (dynamic relaxation) used to solve for the nodal unknowns.

Two separate models are developed in this thesis, one each for the structural solution and the fluid solution. However, the structural solution

depends on the fluid solution and the fluid solution depends on the structural solution. The fourth part of this chapter describes the coupling that must occur between the two solution algorithms for a truly coupled solution.

Tracer information can help immensely when characterizing an HDR reservoir. Though a tracer model is implemented, it was not exercised for this work. The final section of this chapter discusses the tracer solution implemented by Su (1988).

2.1 Element Derivations

This section describes the element derivations for each of the four element types used in this thesis: the two dimensional continuum element, one dimensional fluid flow element, interface element, and boundary spring element. The two dimensional continuum element and interface element derivations follow those of Swenson (1985); the derivation of the fluid flow element follows that of Su (1988). The boundary spring element is a special case of the interface element.

2.1.1 Elasto-Dynamic Structural Element

The equation of equilibrium for a body in three dimensional Euclidean space is

$$\sigma_{ij,j} + b_i = \rho \ddot{u}_i , \tag{2.1}$$

where σ_{ij} is the stress tensor, b_i is the body force, ρ is the density and $\ddot{u}$ is the acceleration ("$\cdot\cdot$" indicates the second derivative of displacement w.r.t. time).

Assuming small displacements, small strains and elastic materials, the strains are related to the displacements by

$$\varepsilon_{ij} = \tfrac{1}{2}(u_{i,j} + u_{j,i}) , \tag{2.2}$$

and the stresses in terms of the strains are

$$\sigma_{ij} = \lambda \varepsilon_{kk} \delta_{ij} + 2\mu \varepsilon_{ij} , \tag{2.3}$$

where δ_{ij} is the Kronecker delta, and λ and μ are Lame's constants.

Multiplying the governing equation 2.1 by a small, arbitrary variation in the displacement, δu_i, and integrating over the volume we have

$$\int_V \sigma_{ij,j} \delta u_i \, dV + \int_V b_i \delta u_i \, dV = \int_V \rho \ddot{u}_i \delta u_i \, dV . \tag{2.4}$$

Integrating the first term of equation 2.4 by parts and applying the divergence theorem gives

$$\int_S t_i \delta u_i \, dS - \int_V \sigma_{ij} \delta \varepsilon_{ij} \, dV + \int_V b_i \delta u_i \, dV = \int_V \rho \ddot{u}_i \delta u_i \, dV , \tag{2.5}$$

where t_i is the surface traction over S and ε_{ij} is the strain tensor.

The finite element approximation for the body is achieved by discretizing the body into elements and applying equation 2.5 to each of the elements. We then sum the contribution of each element to obtain the integrals over the body:

$$\sum_{e=1}^{N} \left\{ \int_{S_e} t_i \, \delta u_i \, dS - \int_{V_e} \sigma_{ij} \, \delta \varepsilon_{ij} \, dV + \int_{V_e} b_i \, \delta u_i \, dV = \int_{V_e} \rho \ddot{u}_i \, \delta u_i \, dV \right\}. \tag{2.6}$$

Introducing matrix notation and working with only one element we have

$$\int_{S_e} \delta \mathbf{u}^T \mathbf{t} \, dS - \int_{V_e} \delta \varepsilon^T \sigma \, dV + \int_{V_e} \delta \mathbf{u}^T \mathbf{b} \, dV - \int_{V_e} \rho \, \delta \mathbf{u}^T \ddot{\mathbf{u}} \, dV = 0 . \tag{2.7}$$

Over each element the displacements are functions of the values at the nodes surrounding the element

$$u = \mathbf{N} \, \mathbf{u}_a, \tag{2.8}$$

where $\mathbf{u}_a$ are the nodal displacements. The strains follow as

$$\varepsilon = \mathbf{B} \, \mathbf{u}_a, \tag{2.9}$$

and the stresses as

$$\sigma = \mathbf{D} \, \varepsilon . \tag{2.10}$$

Using these interpolation functions and substituting into equation 2.7 yields

$$\int_{S_e} \delta \mathbf{u}_a^T \mathbf{N}^T \mathbf{N} \, dS \, \mathbf{t}_a - \int_{V_e} \delta \mathbf{u}_a^T \mathbf{B}^T \sigma \, dV + \int_{V_e} \delta \mathbf{u}_a^T \mathbf{N}^T \mathbf{b} \, dV$$

$$- \int_{V_e} \rho \, \delta \mathbf{u}_a^T \mathbf{N}^T \mathbf{N} \, \ddot{\mathbf{u}}_a dV = 0 . \tag{2.11}$$

Dropping the body force term, and since $\delta \underline{u}_a$ is arbitrary,

$$\int_{S_e} \mathbf{N}^T \mathbf{N} \, dS \, \mathbf{t}_a - \int_{V_e} \mathbf{B}^T \sigma \, dV - \int_{V_e} \rho \, \mathbf{N}^T \mathbf{N} \, dV \, \ddot{\mathbf{u}}_a = 0 . \tag{2.12}$$

Assembling the element contributions, we obtain the global stiffness matrix **K**, the global mass matrix **M**, and the global force vector **f**. The nodal accelerations can now be calculated as:

$$\ddot{u}_a = M^{-1}(f - Ku_a). \tag{2.13}$$

where,

$$Ku_a = \sum_{e=1}^{N} \left\{ \int_{V_e} B^T \sigma \, dV \right\}, \tag{2.14}$$

$$M = \sum_{e=1}^{N} \left\{ \int_{V_e} \rho \, N^T N \, dV \right\}, \tag{2.15}$$

$$f = \sum_{e=1}^{N} \left\{ \int_{S_e} N^T N \, dS \, t_a \right\}. \tag{2.16}$$

Note that $\mathbf{Ku}_a$ is not evaluated as an explicit element matrix multiplied by the displacement vector. It is not even necessary to build a global stiffness matrix. If we place the external forces in a force vector **f**, then accumulate the internal forces from each element's contribution using equation 2.13, we are left with the unbalanced forces that result in the body acceleration.

2.1.2 Fluid Flow Element

Figure 2.1 shows the differential element over which the conservation of mass will be written. The conservation of mass can be stated as,

$$\dot{m}_{in} - \dot{m}_{out} = \frac{d}{dt}(\text{stored mass}), \tag{2.17}$$

or written as,

$$\rho u a l - \left[\rho u a l + \frac{\partial}{\partial x}(\rho u a l)\, dx\right] = \frac{\partial}{\partial t}(\rho a l)\, dx\,, \tag{2.18}$$

where ρ is the density, u is the fluid velocity, a is the crack opening, and l is the element thickness.

For a unit thickness element the volumetric flow rate is q = ua. Now with constant density the conservation of mass can be written as,

$$-\frac{\partial q}{\partial x} = \dot{a}\,. \tag{2.19}$$

Using Darcy's Law we assume that the flow rate is proportional to the pressure gradient and the joint permeability,

$$q = -k_p \frac{\partial p}{\partial x}\,. \tag{2.20}$$

The joint permeability, k_p, is given by the cubic law (Figure 1.3),

$$k_p = \frac{a^3}{12\,\mu\, f}\,, \tag{2.21}$$

where a is the joint opening, μ is the dynamic viscosity, and f is a frictional loss factor. Substituting this into equation 2.19 we get the desired expression,

$$\frac{\partial}{\partial x}\left(k_p \frac{\partial p}{\partial x}\right) = \dot{a}\,. \tag{2.22}$$

We now obtain the weak form of the differential equation by multiplying equation 2.22 by an arbitrary weighting function w and integrating over the joint length,

$$\int_L w\left\{\frac{\partial}{\partial x}\left(k_p \frac{\partial p}{\partial x}\right) - \dot{a}\right\} dx = 0\,. \tag{2.23}$$

Integrating the first term by parts gives,

$$\int_L w\left\{\frac{\partial}{\partial x}\left(k_p\frac{\partial p}{\partial x}\right)\right\}dx = \left[w\,k_p\frac{\partial p}{\partial x}\right]_{L_1}^{L_2} - \int_L k_p\frac{\partial w}{\partial x}\frac{\partial p}{\partial x}dx\,. \tag{2.24}$$

Substituting into equation 2.23 gives the desired result,

$$\left[w\,q\right]_{L_1}^{L_2} - \int_L k_p\frac{\partial w}{\partial x}\frac{\partial p}{\partial x}dx - \int_L w\,\dot{a}\,dx = 0\,. \tag{2.25}$$

The finite element approximation proceeds as before by dividing the joint into discrete elements. The integrals of equation 2.25 are then evaluated over each element and summed over the body,

$$\sum_{e=1}^{N}\left\{\left[w\,q\right]_{L_1}^{L_2} - \int_L k_p\frac{\partial w}{\partial x}\frac{\partial p}{\partial x}dx - \int_L w\,\dot{a}\,dx\right\} = 0\,. \tag{2.26}$$

The first term is the "natural" boundary condition and allows flow rates to be specified where flow rates are not equal to zero.

We introduce shape functions and matrix notation to interpolate the known quantities inside the element,

$$\dot{a} = \mathbf{N}\,\dot{\mathbf{a}}_a,$$

$$w = \mathbf{N}\,\mathbf{w}_a, \qquad \frac{\partial w}{\partial x} = \mathbf{B}\,\mathbf{w}_a,$$

$$q = \mathbf{N}\,\mathbf{q}_a,$$

$$p = \mathbf{N}\,\mathbf{p}_a, \qquad \frac{\partial p}{\partial x} = \mathbf{B}\,\mathbf{p}_a,$$

where **N** is a row matrix of shape functions, **B** is the matrix of the shape function derivatives and $\dot{a}$, $\mathbf{w}_a$, $\mathbf{p}_a$, and $\mathbf{q}_a$ are vectors of the nodal values. Substituting into equation 2.26 yields,

$$\sum_{e=1}^{N} \left\{ \int_{L_e} k_p \mathbf{w}_a^T \mathbf{B}^T \mathbf{B}\, \mathbf{p}_a dx + \int_{L_e} \mathbf{w}_a^T \mathbf{B}^T \mathbf{B}\, \dot{\mathbf{a}}_a dx \right\} = 0 . \tag{2.27}$$

Since $\mathbf{w}_a$ is arbitrary, and the nodal values are constant, we may write,

$$\sum_{e=1}^{N} \left\{ \int_{L_e} k_p \mathbf{B}^T \mathbf{B}\, dx\, \mathbf{p}_a + \int_{L_e} \mathbf{B}^T \mathbf{B}\, dx\, \dot{\mathbf{a}}_a \right\} = 0 . \tag{2.28}$$

Assembling the equations, we obtain the global matrices,

$$\mathbf{K}_p \mathbf{p}_a = \mathbf{Q} - \mathbf{S}\, \dot{\mathbf{a}}_a , \tag{2.29}$$

where $\mathbf{K}_p$ is the permeability matrix, $\mathbf{p}_a$ is the vector of nodal pressures, **Q** is the vector of specified flow rates, **S** is the storage matrix due to the joint openings and $\mathbf{a}_a$ is the vector of joint opening velocities at the nodes. Note that the above formulation recognizes the transient nature of the quasi-steady problem through the rate of the joint displacement. Over each time interval, the total flow in minus the total flow out must equal the change in stored fluid. The transients do not include inertial terms, but arise as changes in flow rates resulting from crack opening velocities.

2.1.3 Interface and Boundary Spring Elements

In this model, where we are approximating rock masses with fractures in them, we need a way to model contact between the rocks and the fracture. The fractures between the rock masses have rough, jagged faces with many small openings and pockets that can contain water long

before the pressures are high enough to cause the joint to open. When the fluid pressures are high enough to overcome the normal stresses in the rock, shear stresses may cause shearing in the fracture before the joint actually opens.

Swenson (1985) included an "interface element" that is implemented as a special case of surface tractions. The term used to apply these tractions is the first term of equation 2.12:

$$\int_{S_e} \mathbf{N}^T \mathbf{N} \, dS \, \mathbf{t}_a,$$

where $\mathbf{t}_a$ are the tractions at the nodes. This element transmits information through a joint to an adjacent element by using a specified traction-displacement relation. Figure 2.2 shows a typical relationship which approximates a rough crack interface (Gangi, 1978). Note that for zero relative normal displacement in the element there is still a traction being applied across the crack. This traction transmits the in-situ stress in the rock normal to the interface element. A shear law is not currently included, however provisions are made so that a law such as that implemented by Asgian (1988) could be implemented in the future. The reader is referred to Swenson (1985) for a complete description of the interface element.

To include the far field stresses in the model, a boundary spring element has been included. This boundary spring represents the characteristics of the far field elastic response. The reservoir is a local (although physically large) perturbation on the rock surrounding the

reservoir. Using the boundary springs allows a small piece of rock to be "cut" out while retaining the elastic effects of the rock outside the cut region. This element is a simple extension of the interface element discussed above. It uses a traction-displacement curve to define a spring stiffness between the boundary of the finite element mesh and the far field. The boundary spring should neither be too soft nor too stiff.

One approximation assumes that the local disturbance decays within a distance the same size as the reservoir. This leads to a stress vs displacement relation given by,

$$\sigma = \frac{\Delta u \ E}{L},$$

where E is the modulus of elasticity, σ is the in-situ stress normal to the spring element, L is the length of the far field rock mass to be modeled as a spring, and Δu is the change in length of the far field rock mass that will completely relieve the in-situ stress. Figure 2.3 shows a typical stress vs displacement relationship used to model the far field stresses.

To implement the finite element method discussed above, the quadratic six noded isoparametric triangle was selected for the structural element (Swenson, 1985), and three node isoparametric line element for the fluid and interface elements. All elements are integrated numerically using Gauss-Legendre quadrature (Zienkiewicz, 1977). Details of the integration for the structure and interface elements can be found in Swenson (1985). The fluid element is similar to the interface element.

2.2 Joint Model

Two of the four element types described in this chapter are used to model the rock joint characteristics as it is pressurized with fluid. The interface element is superimposed on the fluid element to form a pressurized rock joint. The surface tractions due to the fluid pressure are added to the surface tractions due to the interface element. Conceptually this makes sense because initially, when there is no fluid pressure, the rock joint carries all the load. As the fluid pressure increases, according to fundamentals of rock mechanics (Duncan, 1969), the load carried by the rock joint decreases until the fluid pressure is equal to the initial stress in the rock. Using rock mechanics concepts this is stated as:

$$\begin{array}{lcl} \text{Total stress} & = & \underset{\text{(Joint stress)}}{\text{Effective stress}} + \underset{\text{(Fluid pressure)}}{\text{Pore pressure}} \end{array}$$

The pore pressure is simply the fluid pressure and is applied as a surface traction. The effective stress is specified by a stress vs displacement curve that is called the opening law and is also applied as a surface traction. The opening law used in this thesis is the "Bed-of-Nails" model (Gangi, 1978). Gangi showed that the functional dependence of the joint opening variation of a fracture can be modeled as

$$a(P) = a_o\left[1 - \left(P/P_1\right)^m\right], \tag{2.30}$$

where a_o is the zero pressure joint opening, P is pore pressure, P_1 is the effective modulus of the asperities, and m is a constant ($0 < m < 1$) which characterizes the distribution function to the asperity lengths. For all work in this thesis $a_o = 0.32$ mm, $P_1 = 70$ MPa and $m = 0.3636$ (Brown, 1988a).

Figure 2.4 compares the "Bed-of-Nails" model with a "natural" crack. Figure 2.4a shows a "natural" crack formed by creating a hairline fracture, then translating the lower half of the medium to the right. This is similar to how open cracks are formed in nature. Figure 2.4b illustrates the "Bed-of-Nails" model. The distribution of asperities is treated as a distribution of rods, which is much simpler to analyze than the mechanical properties of the natural crack.

The joint law used in the present calculations is very stiff. As a result, it was necessary to use care to ensure convergence. This is discussed in Section 3.1 and Chapter VI.

2.3 Solution Method

As mentioned before, the problem we are solving is highly nonlinear. Many methods exist for solving highly nonlinear problems, but few are as robust as Dynamic Relaxation (DR). Consider a simple problem where a stiffness matrix is a function of displacement. The static equilibrium equation can be written as,

$$\mathbf{K}(\mathbf{x})\,\mathbf{x} = \mathbf{f}, \tag{2.31}$$

where $\mathbf{K}(\mathbf{x})$ is the nonlinear stiffness matrix, $\mathbf{x}$ is the displacement vector, and $\mathbf{f}$ is the force vector. To solve this problem using DR we would rewrite the equation as,

$$\mathbf{M}\,\ddot{\mathbf{x}} + \mathbf{C}\,\dot{\mathbf{x}} + \mathbf{K}\,\mathbf{x} = \mathbf{f}, \tag{2.32}$$

where **M** is a mass matrix and **C** is a damping matrix. If the damping matrix is defined as **C** = c**M**, then equation 2.32 can be rewritten as

$$\ddot{\mathbf{x}} = \mathbf{M}^{-1}(\mathbf{f} - \mathbf{K}\,\mathbf{x}) - c\,\dot{\mathbf{x}} . \tag{2.33}$$

When the mass matrix is lumped to be a matrix with elements on the main diagonal, the inverse of the mass matrix is the inverse of each of the nodal masses. As discussed in Section 2.1.1, an equation of the form of equation 2.33 is vectorizable and does not require that the entire stiffness matrix be assembled. These features greatly reduce storage requirements and simplify programming requirements. Note also that the damping term is a scalar, not a vector or matrix quantity. Equation 2.33 can now be integrated explicitly by the central difference method. The resulting equations are:

$$\dot{\mathbf{x}}_{n+1/2} = \dot{\mathbf{x}}_{n-1/2} + \ddot{\mathbf{x}}_n \Delta t , \tag{2.34}$$

$$\mathbf{x}_{n+1} = \mathbf{x}_{n-1} + \dot{\mathbf{x}}_{n+1/2} \Delta t . \tag{2.35}$$

where n is the time step and Δt is a fixed pseudo-time increment. Now we select Δt, **M**, and c to allow the solution to converge as fast as possible.

The solution algorithm for the structure relies heavily on the original algorithm in Swenson's (1985) code. Because it is a dynamic code, the inertia and physical mass matrix already exist. We alter this original mass matrix to maintain faster convergence. The density for each element is divided by the square of the information transit time for that element.

This has the effect of setting the transit time to ~1 for each element, which also sets the minimum integration time step to ~1. Underwood (1983) shows an example problem that describes this.

For the fluid solution an explicit stiffness matrix is built on the element level. When this is available, Underwood (1983) suggests using Gerschgorin's theorem to make the mass matrix a function of the stiffness matrix:

$$m_{ii} = 1/4\ \Delta t^2 \sum_j | k_{ij} | , \tag{2.36}$$

where m_{ii} are the diagonal elements of the diagonal pseudo mass matrix **M**, and k_{ij} are the elements of the stiffness matrix **K**. He also suggests evaluating **M** with $\Delta t = 1.1$ and iterating with $\Delta t = 1.0$ to ensure stability. Su (1988) found it necessary to iterate at $\Delta t = 0.5$ for stability.

Underwood (1983) also suggests using Rayleigh's quotient to predict the approximate minimum natural frequency ω_o for the current deformation mode,

$$\omega_o = \sqrt{\mathbf{x}^T\mathbf{K}\,\mathbf{x} / \mathbf{x}^T\mathbf{M}\,\mathbf{x}} . \tag{2.37}$$

Then the damping for this mode is approximated by

$$c = 2\,\xi\,\omega_o . \tag{2.38}$$

where ξ is the damping ratio.

The damping ratio ξ can be used to reduce or increase the damping factor for better convergence. Because ω_o is only an approximation to the

lowest active frequency there is only a general correlation between the damping ratio and the rate of convergence.

This method works reasonably well for both the pressure and structure solutions as long as no rigid body modes are present in the solution. Rigid body displacements correspond to low frequencies, and the damping calculated by equation 2.38 becomes extremely small. As a result, higher frequencies are underdamped and convergence is very slow, with much high frequency oscillation. For the problems worked in this thesis rigid body modes are almost always present in both the structure and the fluid. Therefore, an alternate, less sophisticated, but more reliable velocity reduction damping method was implemented. After the accelerations are integrated to update the velocities, the new velocities are multiplied by a reduction or damping term,

$$\dot{x}_{n+1/2} = \left(\dot{x}_{n-1/2} + \ddot{x}_n \Delta t \right) \text{damp} . \tag{2.39}$$

This slowly reduces the velocity as the problem progresses and eventually forces the problem to steady state.

The major problem with this approach is that the appropriate damping is problem dependent. This places a greater burden on the user to examine results closely to ensure convergence. However, due the interactive nature of the program, the analysis can be stopped at any time and the response monitored to allow judgment to dictate whether the damping should be increased or decreased. This allows the user to supply information about how close the solution is to steady state that would

automatically be supplied by a method such as Raleigh's quotient if the rigid body modes were not present.

The value of damping should not be taken lightly however. From equation 2.39 we can see that as $x_{n+1/2}$ is substituted for $x_{n-1/2}$ at each time step the velocities are reduced as a function of C^n where n is the number of iterations. For n = 2000 the effect of damping on the velocity can readily be seen:

Damping	Velocity Reduction
0.999	0.135
0.9999	0.819
0.99999	0.980

From this we can see that small changes in the damping parameter can have profound effects on the solution over several thousand iterations. If the damping factor is increased slightly the velocity reduction will not occur so readily and the solution can progress to convergence at a faster rate. It is the user's responsibility to recognize these inconsistencies while analyzing results and to modify parameters such as the damping factor and tolerance and iteration coupling parameters (discussed in Section 3.1) to ensure that the results obtained are understood thoroughly.

2.4 Coupling between Fluid and Structural Models

As shown above, both the fluid and structural equations are independent modules. The structural model is coupled to the fluid model through the pressures applied on the joints. The fluid model is coupled to

the structural model through the joint opening displacements. In the fluid solution, complete compatibility between the models is obtained. Both the models are solved iteratively. Information is passed between the models at user specified intervals. This process continues until global convergence is obtained.

2.5 Tracer Model

Tracers are used to track the motion of fluid inside an HDR reservoir. Tracer studies can help determine reservoir volume and thermal characteristics as well as other information. At Los Alamos both reactive and nonreactive tracers have been used. Su (1988) developed an uncoupled tracer model for nonreactive tracers. His tracer model has not been exercised in this work, however it is included in the model. Some modifications may be needed before it is used extensively. Robinson (1988) has shown that the joint aperture appropriate for the fluid flow solution may not be appropriate for the tracer fluid flow solution. Figure 2.5 compares the hydraulic aperture w_h with the tracer aperture w_t. The tracer aperture is much larger than the hydraulic aperture used to find the fluid flow solution. The larger aperture for the tracer leads to larger volumes and significantly influences tracer concentrations. Robinson (1985) also developed a residence time distribution curve which is useful for determining a reservoir's volume. His method could be used to verify the tracer model.

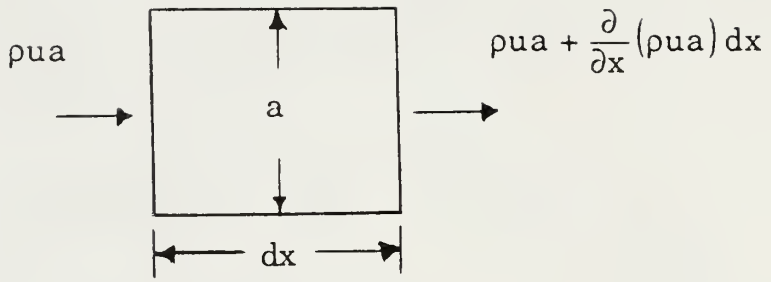

Figure 2.1: Conservation of Mass Differential Element

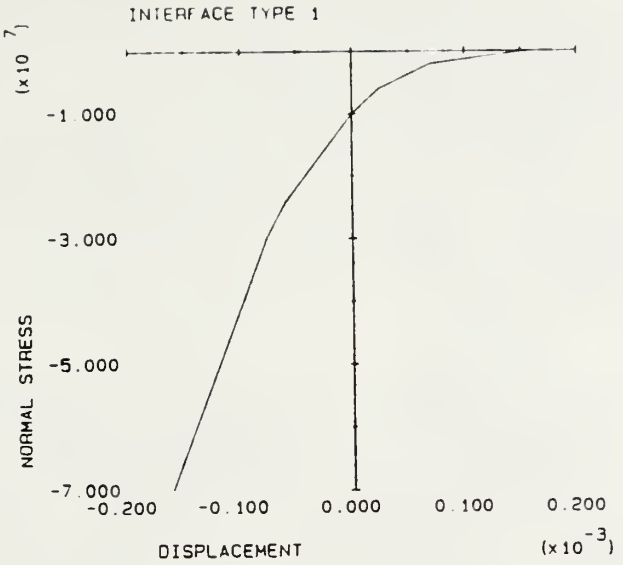

Figure 2.2: Typical Joint Opening Law
Traction -- Displacement Relation

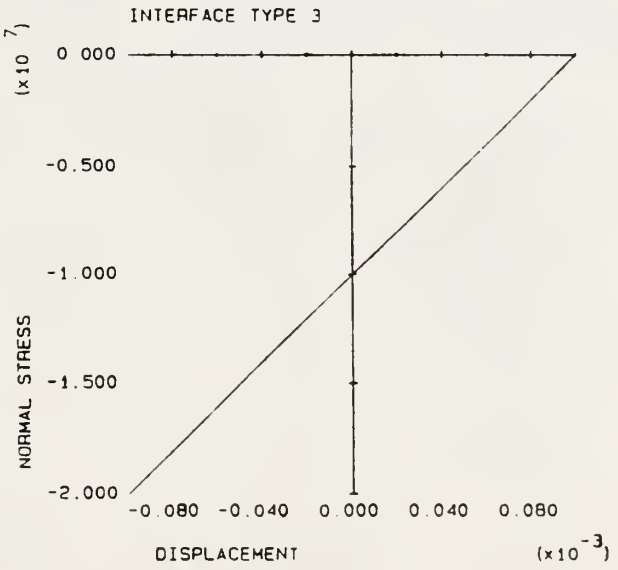

Figure 2.3: Typical Boundary Spring
Traction -- Displacement Relation

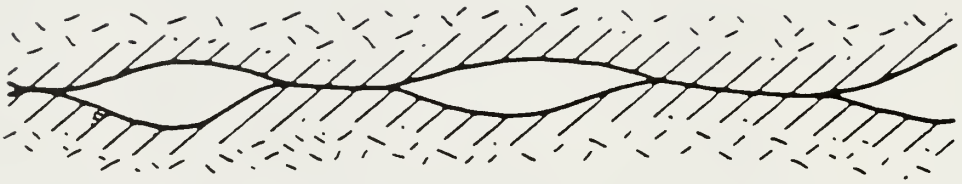

A) Natural Crack (stylized)

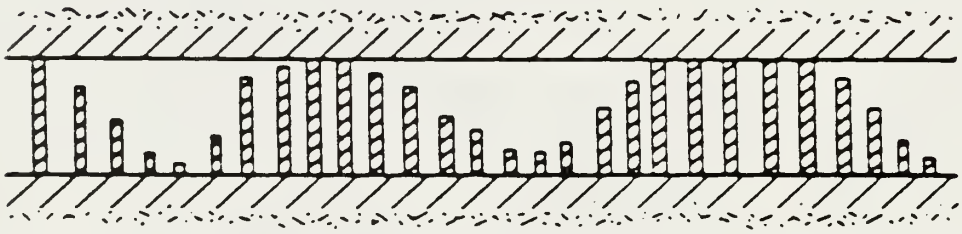

B) Mechanically and Hydraulically Equivalent Crack (schematic)

Figure 2.4: "Bed of Nails" Joint Model
(From Gangi, 1978)

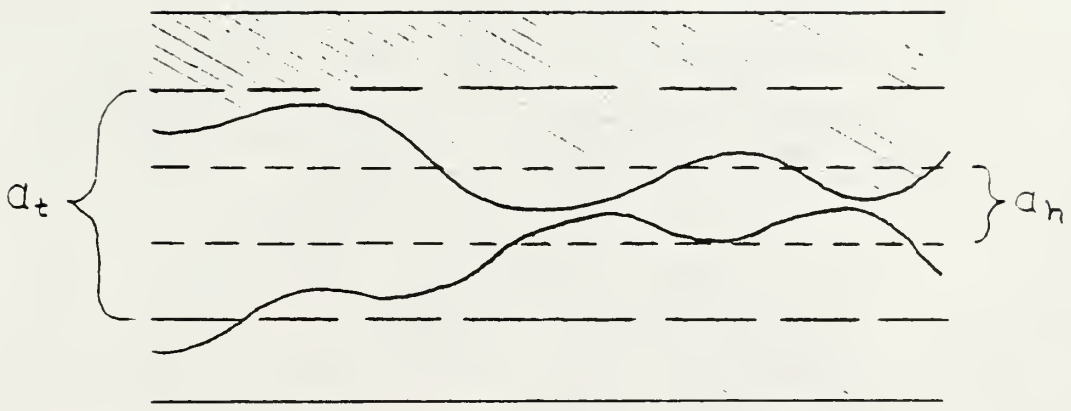

Figure 2.5: Hydraulic Aperture and Tracer Aperture

This page intentionally left blank.

Chapter III

Implementation and Modelling Approach

A computer program called DRACULA (Dry Rock Analysis Code) has been developed to simulate transient fluid flow in fractured, deformable, rock masses. This code implements the equations and concepts discussed in Chapter II. This chapter discusses the basic concepts necessary for operation of DRACULA, then presents some general information about modelling HDR reservoirs.

3.1 Implementation

DRACULA was developed to provide an interactive graphics environment to allow the user to specify and monitor the problem in a simple, reliable way. To monitor the solution's progress, the user can stop an analysis and view intermediate results. If necessary, control parameters can be modified before restarting the analysis. The code CRACKER (Swenson, 1985) was used as a basic foundation to implement these interactive concepts and to make use of the existing structural analysis concepts. The interactive nature of CRACKER unifies the traditionally separate tasks of preprocessing, analysis, and post-processing.

From the MAIN menu page the user may define the problem, save data, run the analysis or view the results (see Fig 3.1). The ANALY PARAM option controls three options: the GLOBAL, FLUID and DYN REL parameter pages. Each of these contains parameters that control program

execution such as end time, time step size, data output frequency and analysis type. The PLOT page allows the user to view the results as pressure and stress contour plots, time history plots, displaced mesh plots and others. SAVE RSTRT, SAVE PLOT and SAVE GEO allow the user to output the restart, plot and geometry data to files for future reference. The REMESH page allows the user to delete and add elements, drag nodes, change material properties, and redefine initial and boundary conditions. GO BATCH and GO INTERACT tell the program to start a batch analysis or perform an interactive analysis. For the batch analysis, a batch start file is written and the program stops, ready to restart in batch mode. For an interactive analysis, as the analysis proceeds messages are displayed to the user in the MAIN PAGE. If trouble is encountered a message is displayed and control returns to the user; in batch mode if trouble is encountered a restart file is written.

Three of the control parameters contained in the DYN REL and FLUID parameter pages regulate the total number of iterations the problem will be allowed to run as well as how often coupling occurs between the two solutions. In the FLUID page the "Number of Fluid coupling iter" is the number of iterations the fluid routine is allowed before it returns the current solution to the structure. In the DYN REL page the "Number of Structure coupling iter" is the number of iterations the structure routine is allowed before it returns the current solution to the fluid. In the DYN REL page the "Total allowed iterations (structure)" is the total allowed iterations for the problem. It is designated for the structure because it actually counts the total iterations for the structure solution. This is because the structure

iterations are more time consuming than fluid iterations. Also, the fluid solution typically converges in less iterations than the structure and can therefore usually have a better fluid solution for every set of structure iterations.

Two other control parameters contained (one each) in the FLUID and DYN REL pages are the convergence tolerances for each of the two routines. The fluid routine uses a different convergence criterion than the structure routine. The fluid routine is converged when each individual normalized pressure change from the last iteration to this iteration changed less than its tolerance:

$$\left| \frac{P_{new} - P_{old}}{P_{old}} \right| < tol .$$

The structure is converged when the square root of the normalized sum of the displacements squared is less than its tolerance:

$$\left(\frac{\sum \left\{ (u_{old} - u_{new})^2 \right\}}{\sum \left\{ (u_{new})^2 \right\}} \right)^{1/2} < tol .$$

In a reservoir there are many fractures that are able to store fluid before building enough pressure to relieve stresses holding the cracks together. To model this phenomenon the fluid elements have a special characteristic -- they are not required to start with fluid in them. If the fluid element's initial opening (a fluid material property) is greater than a user specified tolerance, then the element is assumed to be empty. When adjacent fluid elements fill with fluid they can start to fill the next empty

element, and the fluid solution can progress through the mesh. It is not necessary that any or all of the fluid elements be open, or closed initially. By closing them all, the steady state flow solution for the reservoir can be reached at the end of the first converged solution. By opening them all, the fluid movement through the reservoir can be observed from the time fluid injection begins.

The dynamic relaxation solution method is implemented for both the fluid and structural finite element schemes in separate subroutines. The structure routine solves the structural finite element problem, controls structure data output to files, and controls the coupling between itself and the fluid routine. The fluid routine solves the fluid finite element problem, controls fluid data output to files, and presents the structure routine with an updated fluid solution.

The time step reduction factor is another important parameter contained in the GLOBAL parameter page. The solution method currently implemented is an explicit integration method. The stability of the integration scheme is dependent on the time step size. The solution algorithm will select an appropriate time step based on the size of the smallest structural element, but the stiffnesses of the interface elements and specifically the joint law also need to be considered. Because the joint law is very stiff compared to a typical structural element for these problems, the time step must be reduced by a factor of 100. This increases the run time on a problem because 100 times as many time steps are now

required for the same displaced solution. Chapter VI gives recommendations on removing this constraint.

3.2 Modelling Approach

HDR reservoirs are large, three dimensional underground regions, typically measured in hundreds of meters. These three dimensional regions comprise a lattice of small and large fractures. When fluid is pumped into a reservoir the reservoir expands like a balloon. Most of the fluid can be recovered by letting the reservoir contract, but some of the fluid will be lost at the outer boundary of the reservoir and some is trapped in "open" fractures. The Phase II HDR reservoir at Fenton Hill, New Mexico displays these characteristics. As a first approximation the Phase II reservoir will be modelled as a horizontal plane with unit depth. We look at the horizontal plane in plan view, with flow occurring only in the fractures in this plane.

The researchers at Los Alamos National Laboratory have evidence that as 99% or more of the volume in their HDR reservoir is due to the small, low opening stress fractures (Brown, 1988). A small number of the fractures in the reservoir have a high opening stress. The low opening stress fractures are called "tensile" fractures, and the high opening stress fractures are called "shear" fractures. Brown (1988) also reports that the principal stresses on the reservoir are about 10 MPa and 24 MPa for the minimum and maximum principal in-situ stresses. For this model the shear fractures are assumed to be perpendicular to the maximum principal stress and the tensile fractures are assumed to be perpendicular

to the minimum principal stress. In reality the principal stresses would be rotated counterclockwise slightly, but DRACULA does not currently have a shear law in the joint model. The in-situ stress on the tensile fractures is 10 MPa, and the in-situ stress on the shear fractures is 24 MPa; both are strictly normal stresses.

3.2.1 Joint Model Implementation

As discussed in Section 2.2, the joint model uses the fluid element superimposed on the interface element. The tensile fractures and shear fractures use the same joint model but refer to different materials. The tensile fractures use material type one; the shear fractures use material type two. The fluid and interface elements get their material data from their respective material tables. Figure 3.2 shows the joint opening law for interface types one and two. There is only one opening law as defined in Section 2.2. The curve is shifted to keep the body in initial equilibrium for the two in-situ stresses. The distance the curve is shifted must be stored as fluid material data to be used as an initial opening for the joints. This gives each joint some finite free volume before any fluid is pumped in.

Figure 3.3 shows the finite element mesh used for the problems analyzed in Chapter IV. The three vertical joints model the shear fractures. The tensile joints are offset to force the flow paths to include the high opening stress shear joints.

3.2.2 Reservoir Boundary Conditions

To model the effects of the rock surrounding the reservoir, springs are placed on the outer edge of the finite element mesh. Figure 3.4 shows typical plots for interface materials three and four. Notice that the springs are preloaded to 10 MPa and 24 MPa to maintain initial equilibrium. As the reservoir expands and the volume increases the far field stress increases with the spring's compression. The spring element sets the displacements on the outside of the element to zero and has inside nodes attached to the rock masses.

The fluid boundary conditions are important to consider before running a problem. Pressure and flow rate histories may be specified for transient problems. The "natural" boundary condition for the fluid flow problem is that no flow occurs on a boundary where no condition is specified. One other condition that can be applied globally to the reservoir boundary is a condition that allows fluid to "leak" out of the reservoir as a function of flow rate vs. pressure. This is called a far field flow loss or leakage boundary condition.

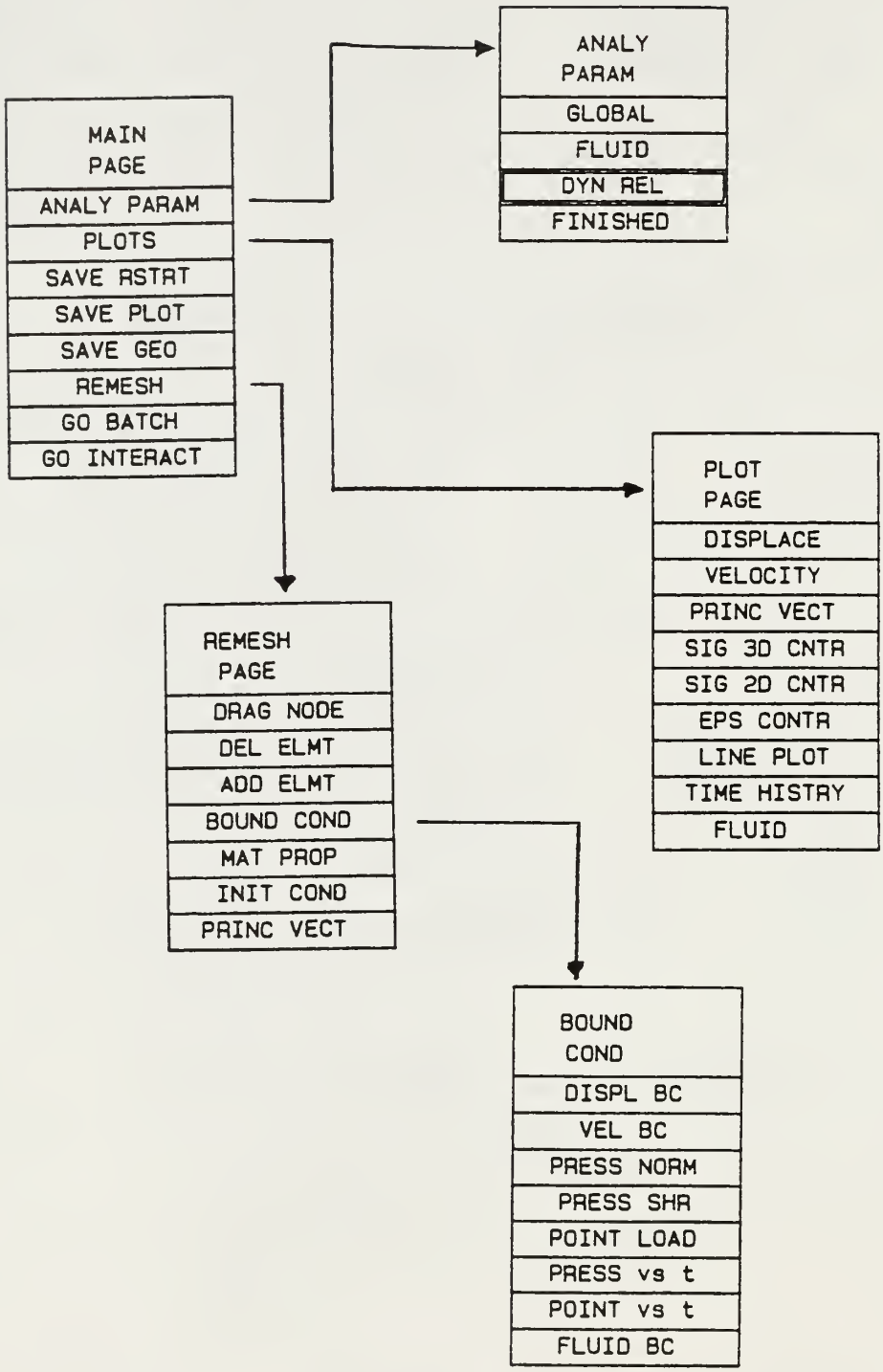

Figure 3.1: DRACULA Menu Concept

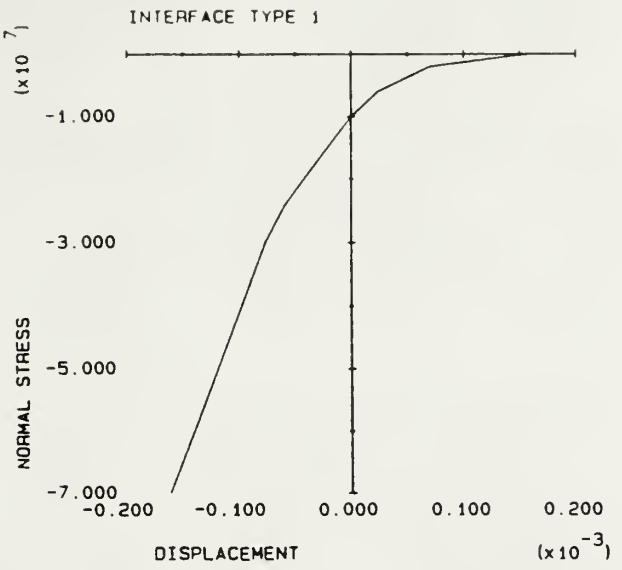

a) Y Displacement -- Traction Relation

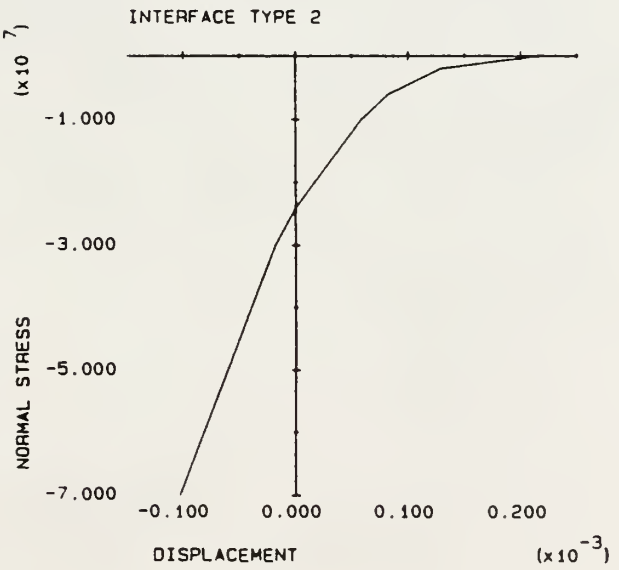

b) X Displacement -- Traction Relation

Figure 3.2: Joint Opening Law,
Interface Materials One and Two

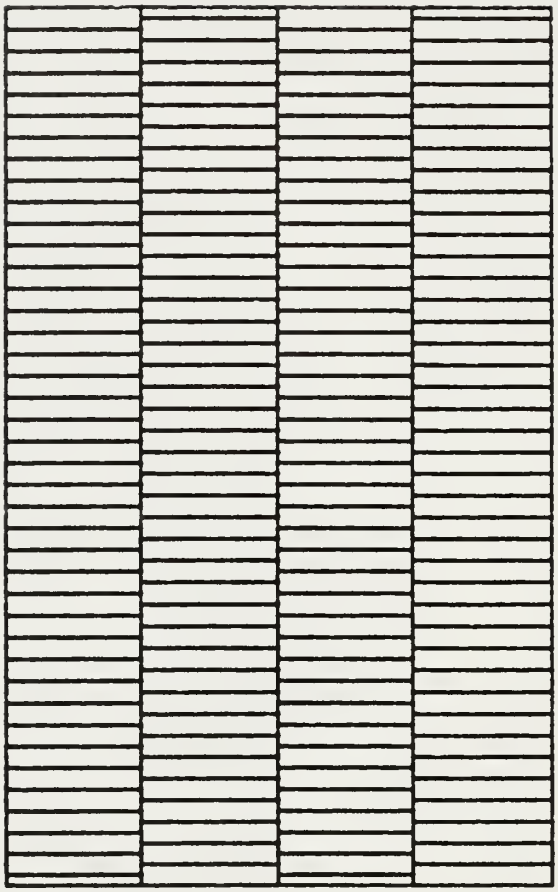

Figure 3.3: Application Problems Finite Element Mesh
(Note: Only flow paths shown for clarity)

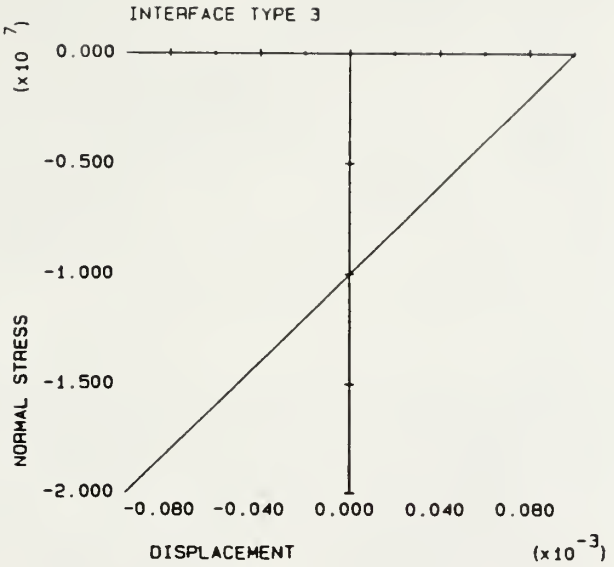

a) Y Displacement -- Traction Relation

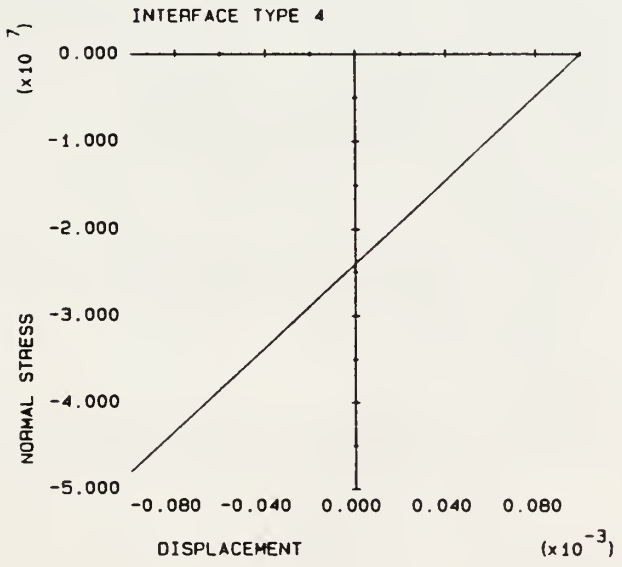

b) X Displacement -- Traction Relation

Figure 3.4: Boundary Springs,
Interface Materials Three and Four

Chapter IV

Verification Problems

Two verification problems will be used to illustrate DRACULA's ability to model fluid flow. A single flow path is used so the results can be interpreted more easily. The path considered is one tensile flow path from Figure 3.3. The first problem is a steady state flow problem. A specified flow rate is applied at one boundary of the problem and a far field flow boundary condition is applied to allow fluid leakage at the other boundary. The second problem is a transient flow problem. A constant reservoir pressure is applied and the steady state (no fluid flow) solution is found. Then a step change in the pressure boundary condition initiates a pressure transient.

Figure 4.1 shows the mesh used for both of the problems discussed in this chapter. The verification problems are simple, one dimensional problems with a single flow path in the X direction. Table 4.1 summarizes the reservoir properties used for all the problems in this thesis. Poisson's ratio was set to zero for the verification problems. Figure 4.2 shows plots of the boundary spring stiffness applied for both verification problems. Boundary springs with a relatively high stiffness were used to help speed convergence.

4.1 Steady State Verification Problem

This problem displays the option to specify a pressure - flow rate relation on the boundary of the mesh to simulate a far field "leakage"

boundary condition. Figure 4.3a shows the far field relation specified as a linear function of pressure and flow rate (nonlinear functions can also be specified). The flow rate was specified at the right end of the mesh as shown by Figure 4.3b. Normally the far field pressure - flow rate relation would be enforced on the right boundary as well as the left boundary. But when a specific pressure or flow rate condition is specified on a boundary, the far field boundary condition will not be applied at that node.

The flow rate solution should be constant through the entire flow path. Also note that numerically all the boundary conditions specified for this problem are flow rates; however, because the far field boundary condition is a function of pressure, a unique pressure solution does exist. Convergence rates are normally slower for problems with far field and flow rate boundary conditions specified.

Figures 4.4 is a flow rate plot for this steady state problem. The flow rate is constant through the flow path as expected. As shown by Figure 4.5, the pressure on the left boundary corresponds to the correct flow rate for the far field boundary condition. In addition, the joint stress shown by Figure 4.6 added to the fluid pressure from Figure 4.5 gives the total stress shown by the line plot of the Y stress in Figure 4.7. This shows that the fundamental rock mechanics assumption from Section 2.2 is satisfied in DRACULA.

The last figure for this problem (Figure 4.8) is a displaced mesh plot. Note that the joint openings change as the pressure changes in the joint.

Since the flow rate is constant through the flow path, the pressure gradient must also adjust with the joint openings to maintain the specified flow rate.

4.2 Transient Verification Problem

This problem is analogous to inflating a balloon. All the input flow is used to expand the joint. If the pressure is reduced, this stored fluid is available to flow out of the joint. To start the problem a constant 9.0 MPa fluid pressure was applied to one end of the flow path and a zero flow boundary condition was imposed on the opposite end of the flow path. This results in a fluid solution with constant fluid pressure in the joint and no fluid flow. Next the applied pressure is dropped to 1.0 MPa, initiating a pressure transient in the problem, causing fluid flow out of the joint.

The analytical solution for the first part of this problem comes from a simple one dimensional rock compression problem. The fluid pressure is constant in the joint, causing a uniform linear translation of the two rock masses. The initial stress in the block is σ_x = -24 MPa and σ_y = -10 MPa. Initially the joint also has a stress of -10 MPa. Inflating the joint to a fluid pressure of 9 MPa opens the joint. This causes the block to translate and increases the boundary load to -10.2 MPa. In the joint, the fluid pressure is 9 MPa and the joint stress is reduced to 1.3 MPa. The stress in the block also increases to 10.3 MPa. The values are not exact because relatively loose convergence tolerances were used. The effect of this can be seen on the line plot in Figure 4.9. The Y stress should be constant along this line plot. Figure 4.10 is a time history plot that also shows that though the solution is

nearly converged, more iterations are needed to allow the blocks to translate and increase the boundary spring load to -10.3 MPa.

At time = 0^+ the applied pressure was dropped to 1.0 MPa. Each transient solution must be obtained by iterating on the nonlinear flow problem, with the previous solution giving initial conditions for the solution currently being sought. An important parameter that must be selected before a transient is initiated is the time step (t-step) over which the transient will act. Recall from Chapter II that the fluid flow is governed by,

$$\mathbf{K}_p \mathbf{p}_a = \mathbf{Q} - \mathbf{S}\,\dot{\mathbf{a}}_a.$$

The $\mathbf{S}\,\dot{\mathbf{a}}_a$ term acts as a fluid source in the analysis. If a joint is closing, this term supplies additional flow to the calculation. In DRACULA the $\dot{\mathbf{a}}_a$ term is implemented in finite difference form as,

$$\dot{\mathbf{a}}_a = \frac{\mathbf{a}_{new} - \mathbf{a}_{old}}{\text{t-step}}.$$

The fluid flow equations we are solving are now a linear function of the joint displacements from the mesh ($\mathbf{a}_{new}$) and still a cubic function of joint displacements in the joint permeability. The flow rates are influenced directly by the selection of t-step as well as the displacements. Notice above that as t-step increases, the storage term has less and less effect on the solution, and approaches the steady state solution. And conversely, as t-step is reduced, the flow rates can be influenced significantly by the storage term.

Figure 4.11 shows a time history of four displaced mesh plots for a transient solution with t-step = 0.125. As shown in Figure 4.12, the initial condition at time = 0.0 is a uniform joint opening with a pressure of 9.0 MPa. When the pressure at the outlet is dropped, fluid begins to flow out of the joint. The joint closes first at the outlet. Eventually, the excess fluid is forced out of the joint and the pressure is uniform at 1.0 MPa.

Figure 4.14 is a history plot of the fluid flow rate at the outlet and a history plot of the pressure at the opposite end of the flow path. The outlet flow rate rapidly decreases as the pressure driving the flow decreases to the specified outlet pressure.

Figure 4.15 is a similar fluid flow rate plot comparing the outlet flow rate for different values of t-step. This plot displays the effects t-step has on the storage term as discussed above. Smaller values of t-step cause higher initial flow rates with sharper transients; larger values of t-step cause lower initial flow rates with solutions nearer a new steady state solution for the new boundary condition.

One simple check for the validity of a transient solution for this type of problem is that the integral over time of the flow out of the joint be equal to the change in volume of the joint. Table 4.2 summarizes the changes in volume representing the integrals for the area under each flow rate vs. time curve from Figure 4.15. As t-step decreases from 0.5, the volume integrated under the flow rate curve approaches the actual change in volume. Note that for t-step = 1.0 the integrated volume is also increasing

and approaching the actual change in volume. As the time step is increased the solution does approach the next steady state solution.

4.3 Summary

In this chapter we presented two verification problems to illustrate DRACULA's ability to model coupled fluid flow and rock deformation in an HDR reservoir. The first problem displayed steady state results from flow rate and far field fluid boundary conditions. The finite element results show that the flow rate is constant through the flow path at the correct specified value and that the pressure solution does satisfy the far field boundary condition. The second problem showed the effects of the time step size on the results of a transient solution. This problem shows that the time step size does affect the results of a transient problem and that as the time step size is reduced a more accurate transient solution is obtained. Both problems show that the effective stress law from Section 2.2 is satisfied.

Table 4.1

Reservoir Properties

Poisson's Ratio	0.20
Young's Modulus	25000 MPa
Initial Joint Aperature, x	0.1032e-3 m
Initial Joint Aperature, y	0.1632e-3 m
Maximum Principal Stress, σ_x	24 MPa
Minimum Principal Stress, σ_y	10 MPa
Fluid Dynamic Viscosity, μ (@ 220° C)	116.6e-6 N-s/m^2
Factor of Roughness, f	1.5

Table 4.2

Joint Volume Change

t-step (s)	0.0625	0.125	0.25	0.5	1.0	∞
Vol. (m^3x10^6)	933.5	925.9	916.5	914.7	947.3	957.9

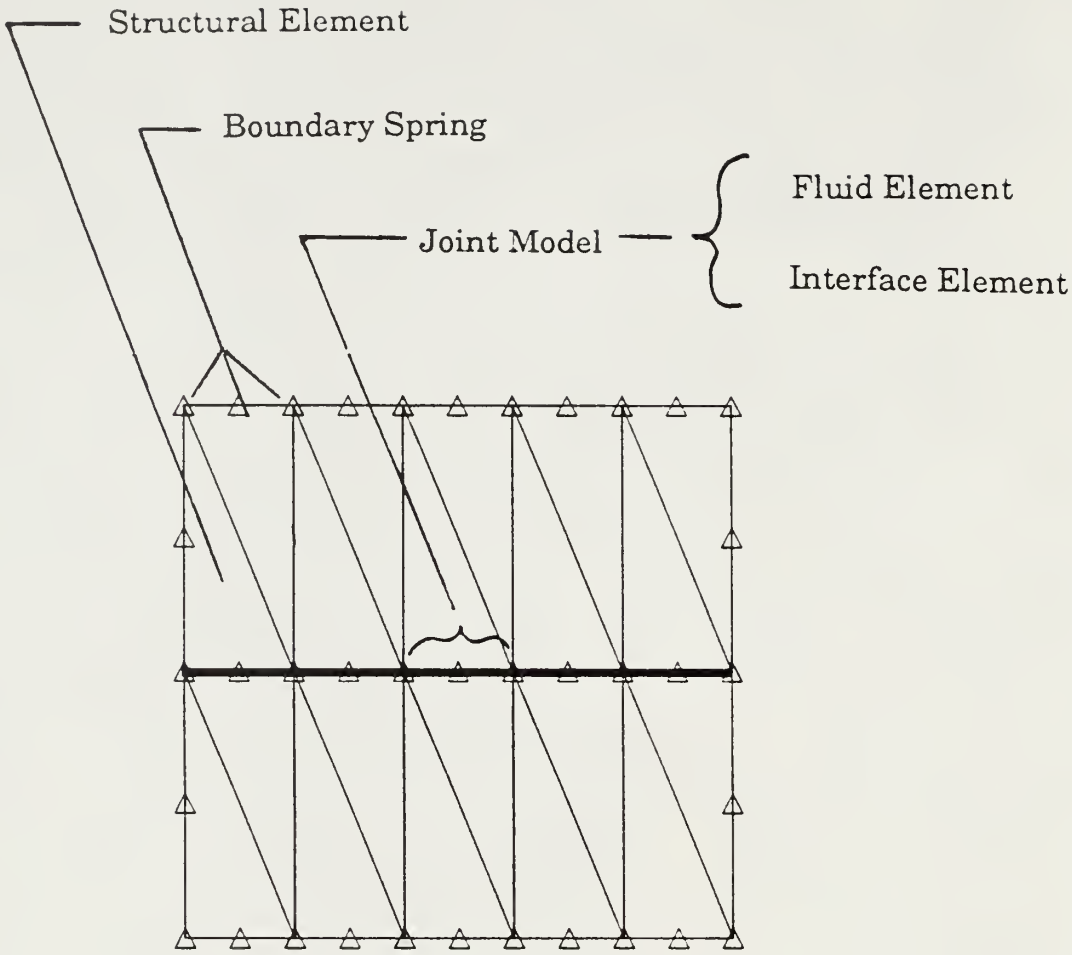

Figure 4.1: Verification Problems Finite Element Mesh

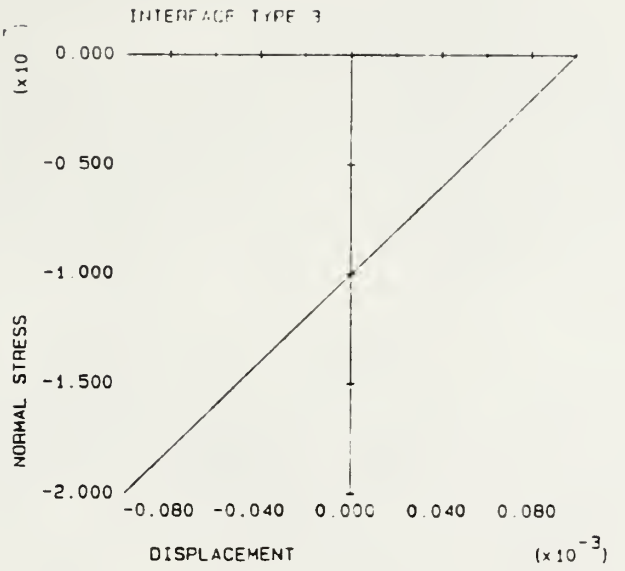

a) Y Displacement -- Traction Relation

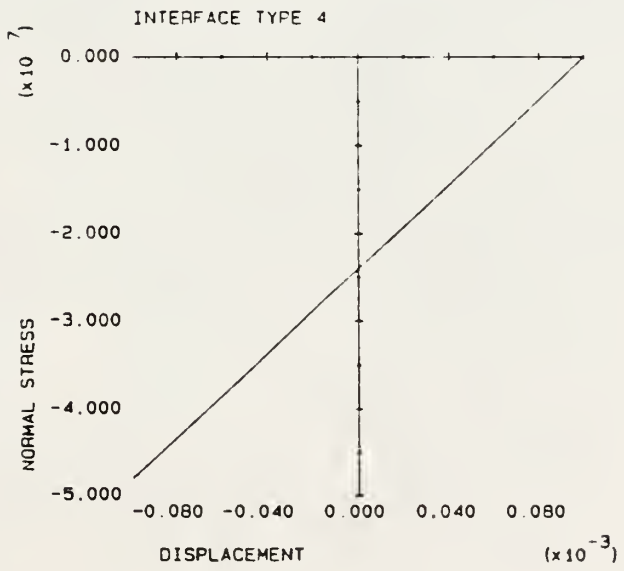

b) X Displacement -- Traction Relation

Figure 4.2: Verification Problems Boundary Springs

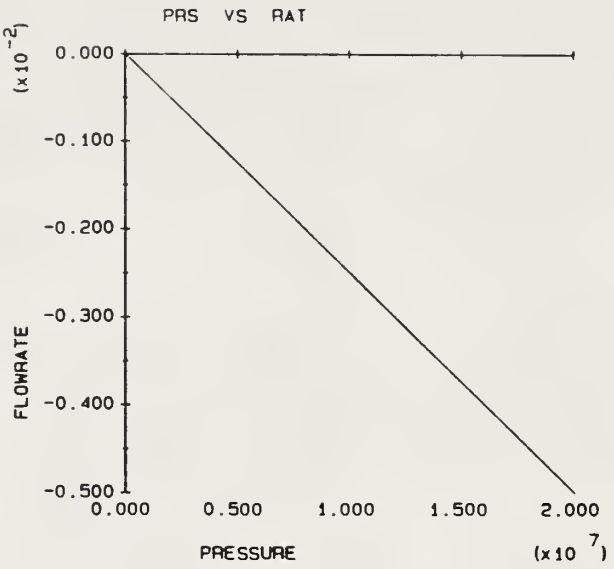

Figure 4.3a: Far Field Flow Loss Boundary Condition (Steady state verification problem)

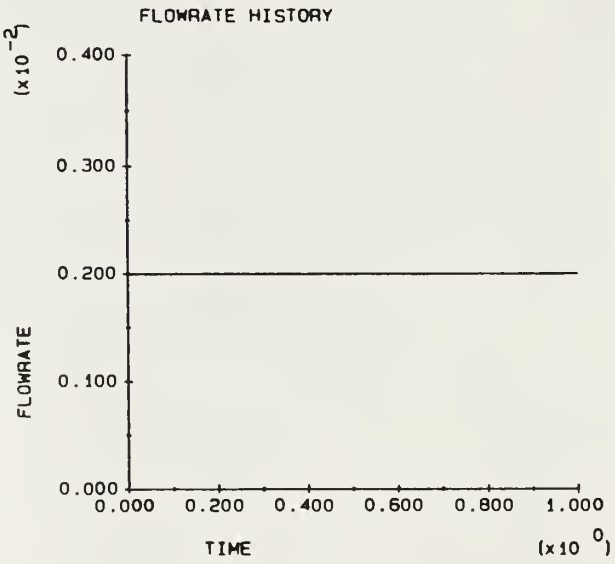

Figure 4.3b: Flow Rate Boundary Condition (Steady state verification problem)

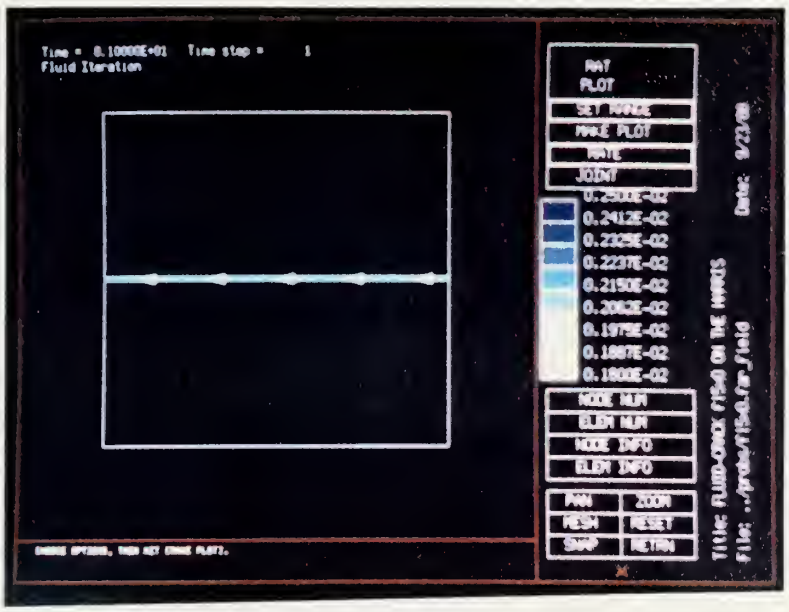

Figure 4.4: Flow Rate Contour Plot
(Steady state verification problem)

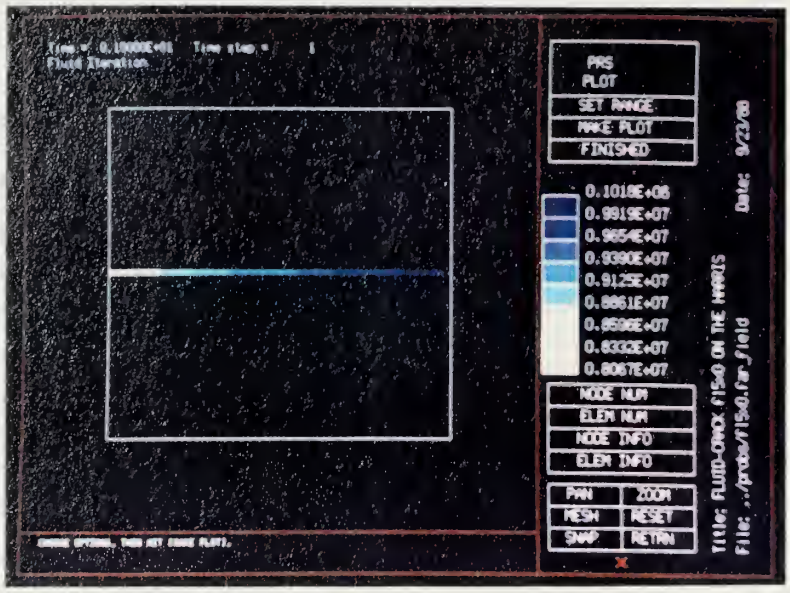

Figure 4.5: Pressure Contour Plot
(Steady state verification problem)

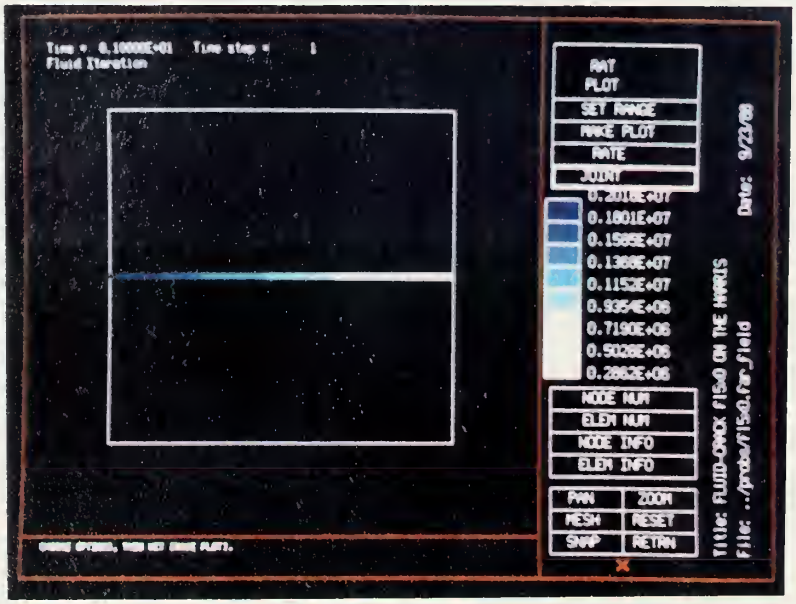

Figure 4.6: Joint Effective Opening Stress
(Steady state verification problem)

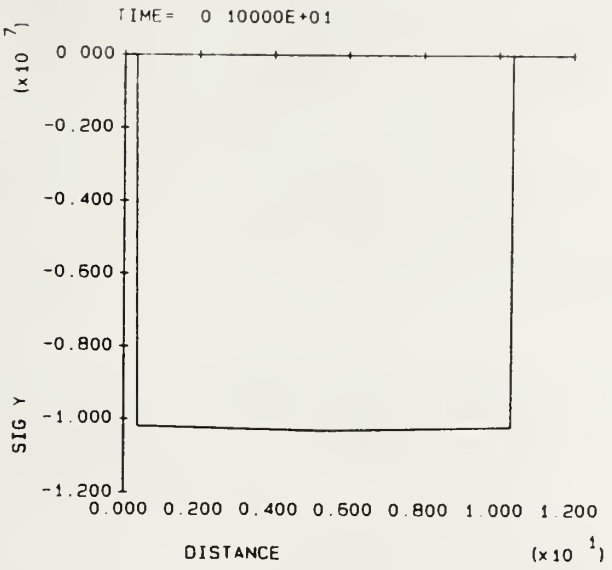

Figure 4.7a: Y Stress Line Plot
(Steady state verification problem)

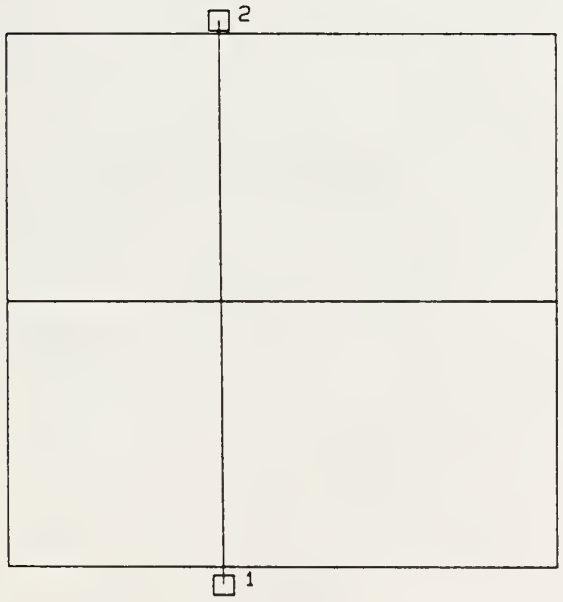

Figure 4.7b: Line of Application for Above Line Plot

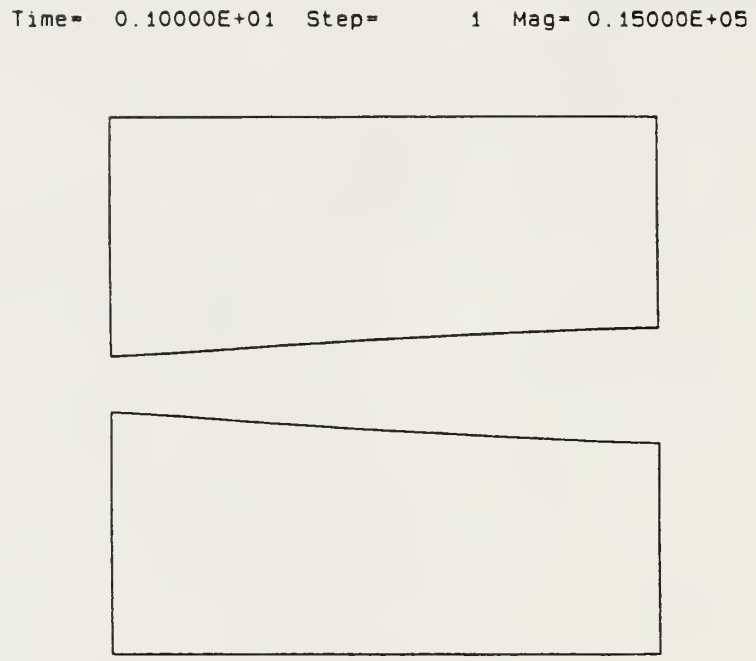

Figure 4.8: Displaced Mesh Plot
(Steady state verification problem)

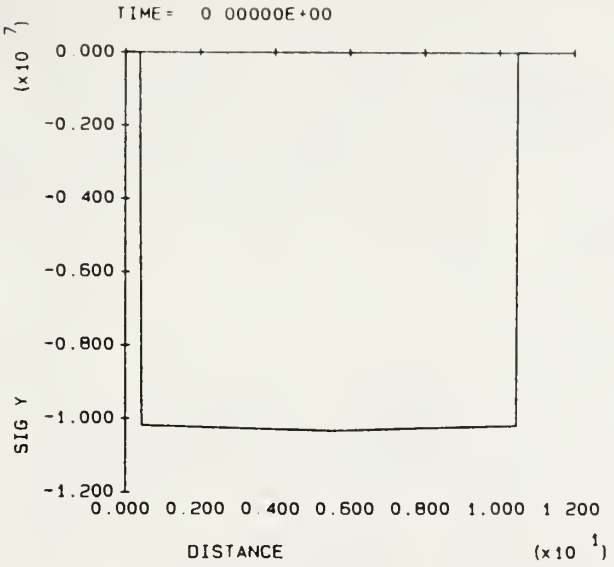

Figure 4.9a: Y Stress Line Plot, time = 0.0
(transient verification problem)

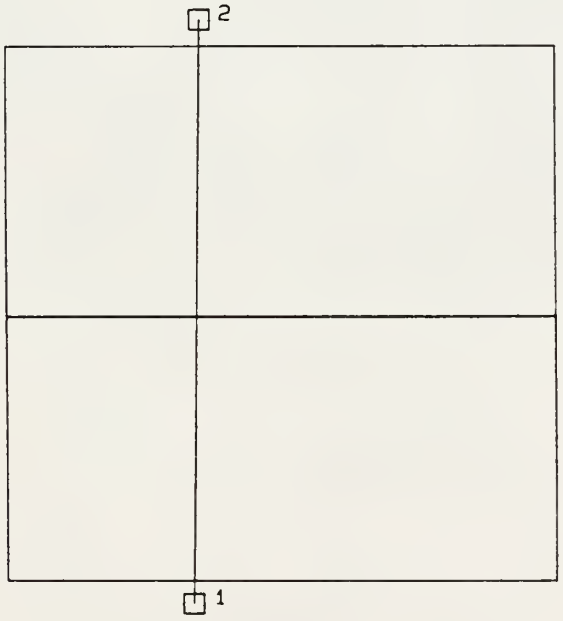

Figure 4.9b: Line of Application for Above Line Plot

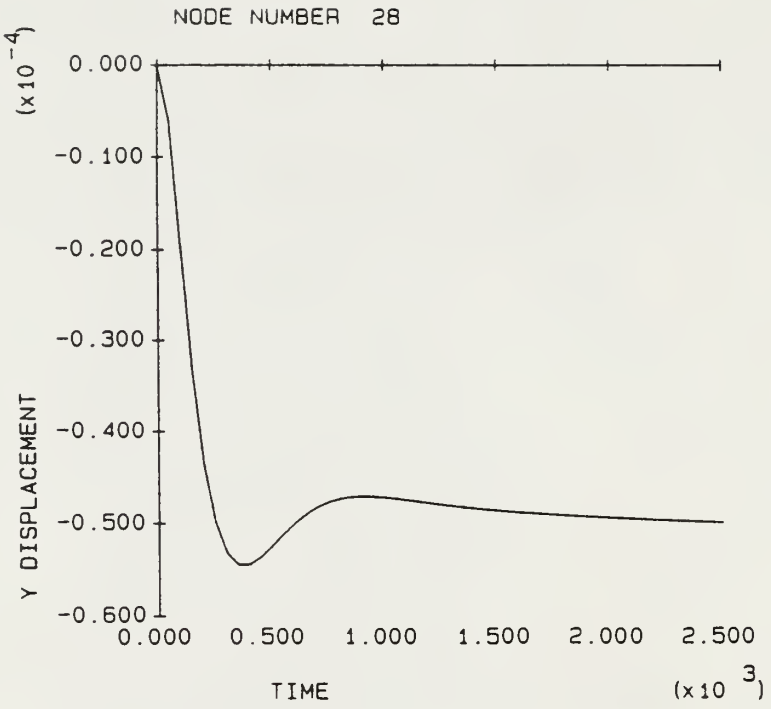

Figure 4.10: Time History Plot, Initial 9 MPa Solution (transient verification problem)

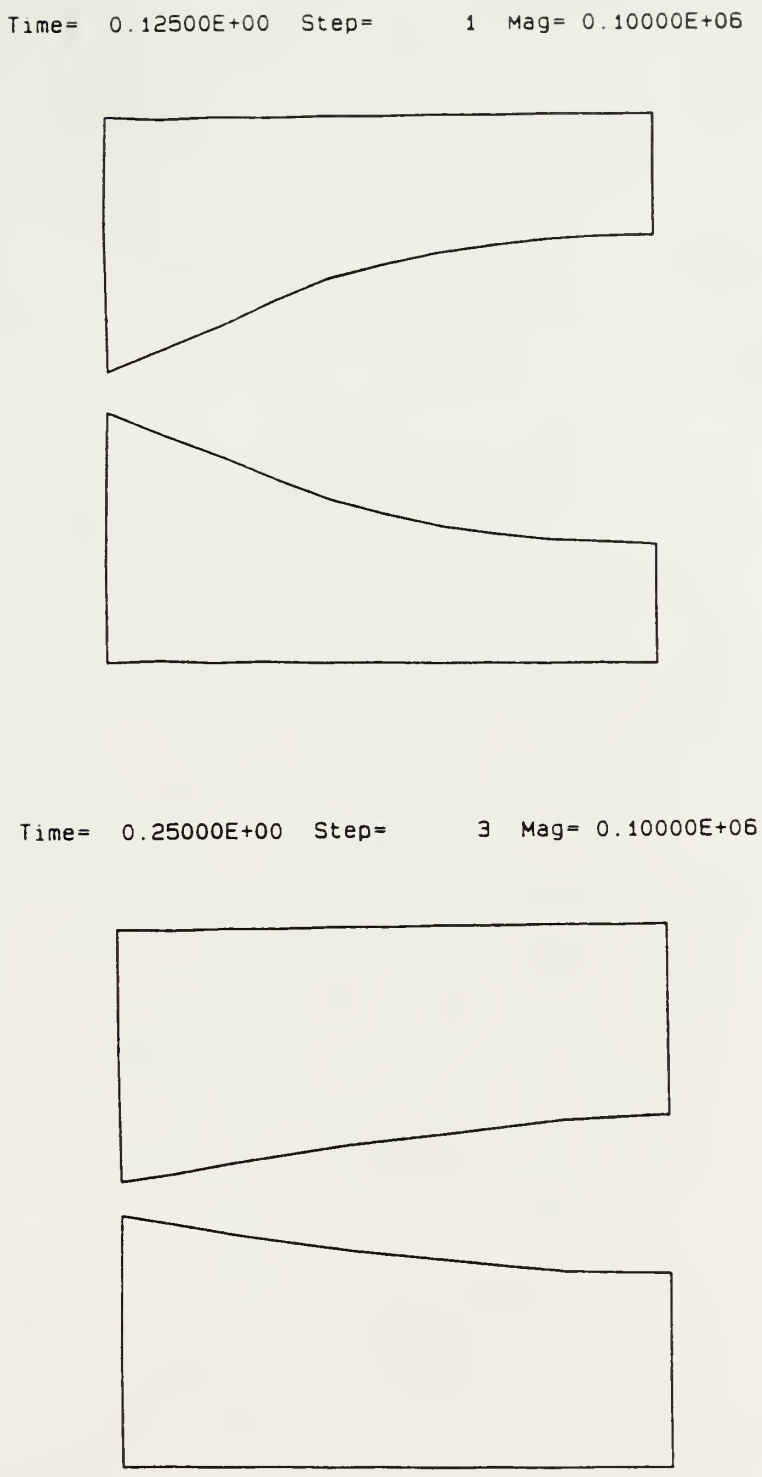

Figure 4.11: Time History Plot of Displaced Mesh Plots, t-step = 0.125 (transient verification problem)

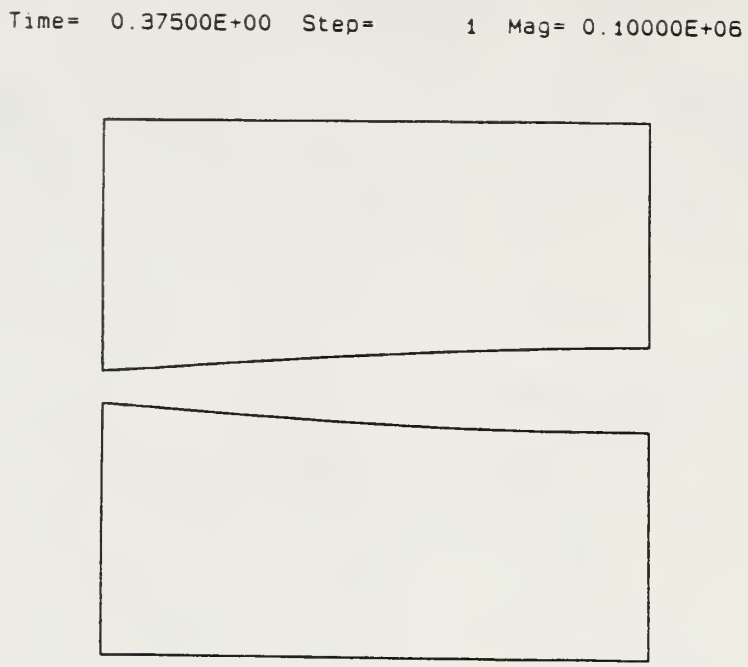

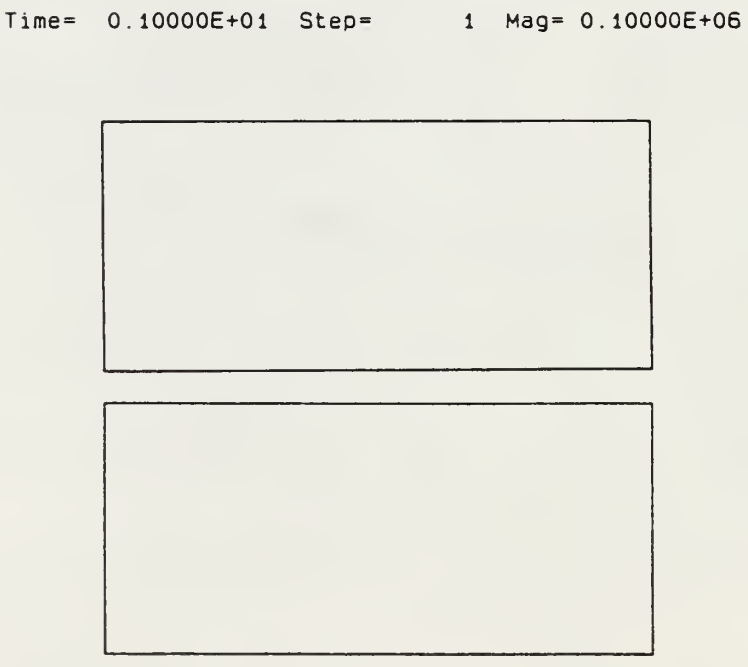

Figure 4.11 cont: Time History Plot of Displaced Mesh Plots, t-step = 0.125 (transient verification problem)

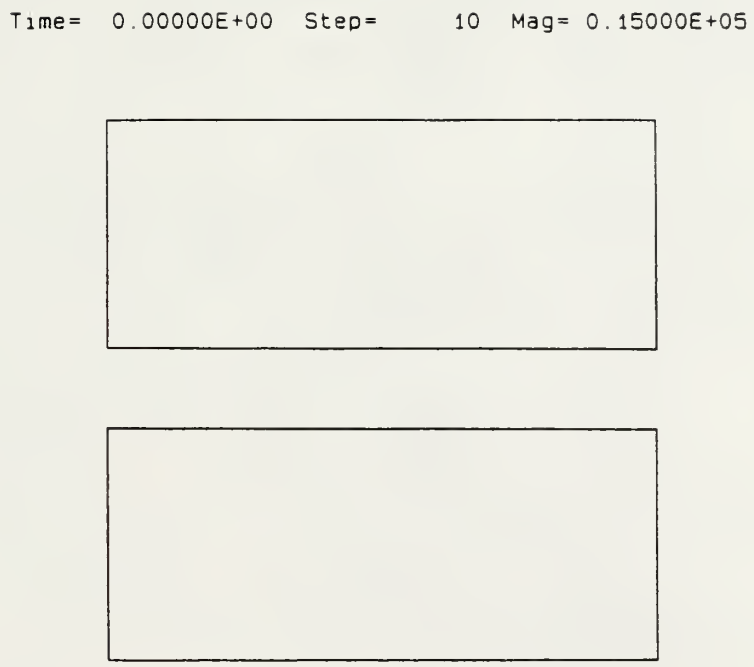

Figure 4.12: Initial Displaced Mesh Plot
(transient verification problem)

Figure 4.13: This figure intentionally left blank

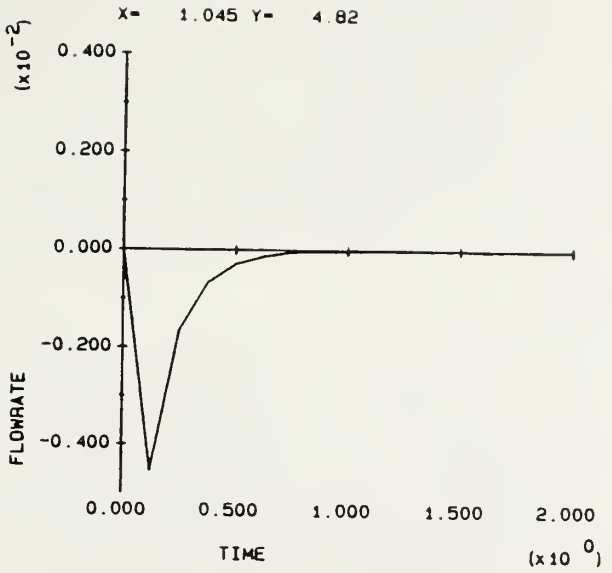

Figure 4.14a: Flow Rate Transient Solution
(transient verification problem)

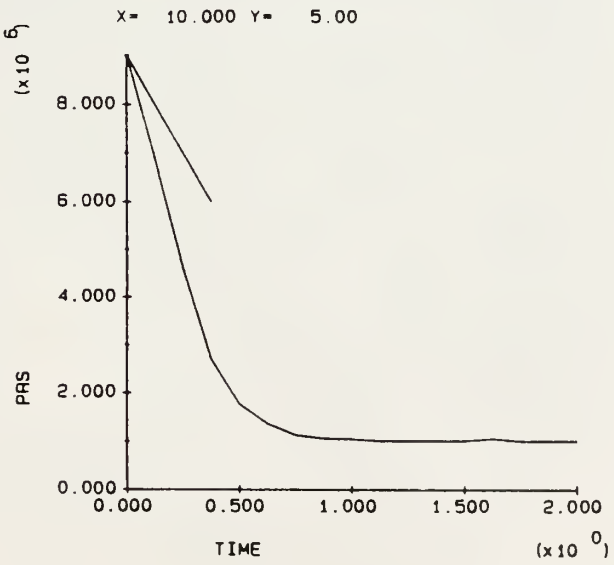

Figure 4.14b: Pressure Transient Solution
(transient verification problem)

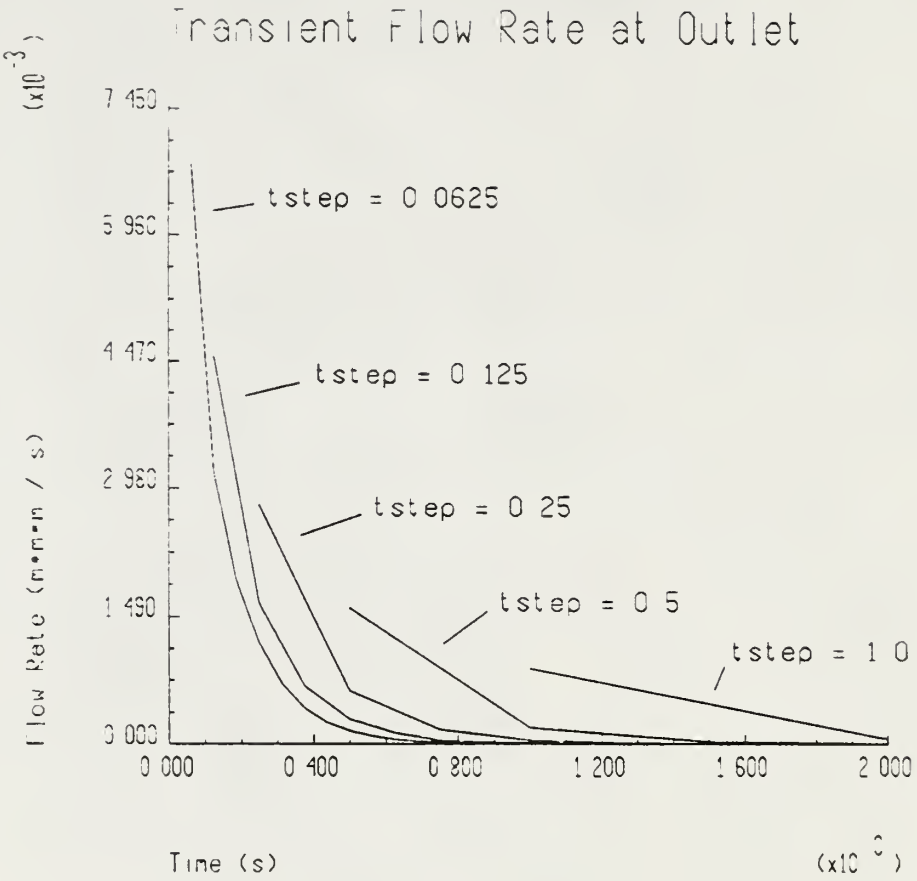

Figure 4.15: Fluid Flow Rate Solution for Different values of t-step (transient verification problem)

Chapter V

Applications

This chapter presents the results of several problems analyzed to investigate the transient and steady state flow characteristics of an HDR (Hot Dry Rock) reservoir. Each of the problems presented here use the same finite element mesh. The first two problems are steady state flow problems. Fluid is not allowed to leak at the mesh (reservoir) boundary for either problem. One problem has the injection well fluid pressure lower than both in-situ reservoir stresses; the other problem has the injection well fluid pressure above the minimum in-situ reservoir stress, but lower than the maximum in-situ reservoir stress. The last problem has transient boundary conditions that model experiment #2070 conducted by Los Alamos National Laboratory at Fenton Hill, New Mexico. It applies a pressure history at the injection well (EE-3A) and monitors the pressure rise at the shut-in extraction well (EE-2). There is no far field fluid leakage.

5.1 Low Pressure Steady State Problem

Figure 5.1 shows the mesh used for this steady state problem with the boundary conditions labelled. Problems with only pressure boundary conditions converge more rapidly than those with other boundary condition types. For this problem, with two pressure boundary conditions, both below the minimum in-situ stress, none of the joints will completely open and the joint law will remain in effect.

Figure 5.2 is a fluid pressure contour plot showing the steady state pressure solution. The pressure plot is almost perfectly symmetric about a vertical center line through the mesh with little pressure drop in the X direction and a nearly linear pressure drop in the Y direction. The flow rates through the mesh are shown in Figure 5.3. The arrows represent flow direction when shown on the plot. The arrows are not shown for flow rates out of the legend range. The flow rates are constant and the same for each of the three vertical flow paths. The extremely small flow rates on the boundaries indicate that the fluid solution is converged reasonably well for the current structure solution. A careful investigation of the flow rates at the extraction well shows that some flow does move around behind the extraction well to exit the mesh (see Figure 5.4).

Figure 5.5 is a displaced mesh plot for the steady state flow solution. Notice that the higher fluid pressures at the bottom of the mesh near the injection well cause both horizontal and vertical joints to open more than at the top of the mesh. Also notice that the stiffer vertical joints are not as far open as the softer horizontal joints, as predicted by the difference in the joint opening laws for the two. The pressure drop is low enough across the soft tensile joints that they provide a constant pressure "header" across the bottom of the mesh.

Throughout the mesh the displacements are not as uniform as the pressure plot might indicate. This is because the problem is not completely converged. To reduce computer run times a loose structural solution tolerance was used. An inspection of the displacement history plots for

several nodes in the mesh shows that run times were reduced at the expense of totally converged solutions. Figure 5.6 compares X and Y displacement history plots for three nodes in the mesh. Each of the X displacement plots show good convergence, as expected from the displaced mesh plot. The Y displacement history plots do not show good convergence even though the specified tolerance was met. However, the solution is nearly converged. The line plot in Figure 5.7 shows the Y stress varies only slightly in the mesh from the top to the bottom and is near the expected value. As discussed in Section 3.1, the relatively slow convergence is due to the extremely stiff joint law that forced a time step reduction of 100. A solution to this difficulty is discussed in Chapter VI.

5.2 High Pressure Steady State Problem

This problem has specified pressure boundary conditions in the same locations as the previous steady state problem. For this problem the injection pressure is 15 MPa and the extraction pressure is still 1 MPa. When the fluid pressure rises above the initial in-situ stress the joint elements will open and not carry any load. Only the fluid pressure in the joints will act on the rock blocks, which can "float" in the middle of the mesh. The blocks are free to move because with only the fluid pressure acting, translations are possible without changes in the force balance. As fluid pressures continue to rise and the joint openings increase, the blocks are free to translate more.

In this problem we demonstrate the ability to model floating blocks by specifying in inlet pressure of 15 MPa and an outlet pressure of 1 MPa.

Because the inlet pressure is above the minimum in-situ stress of 10 MPa in the Y direction, joints will completely open and blocks will "float" in the Y direction near the inlet.

Figure 5.8 shows the calculated pressure distribution. A uniform pressure does exist locally around the inlet location. This is because the joints have completely opened and all load is being carried by the fluid in the joints. As we approach the outlet, the pressure decreases and the structural joints are carrying part of the load.

To satisfy equilibrium, the final stress in the Y direction should be 15 MPa, consistent with the specified input pressure. Figure 5.9 is a line plot of the Y stress in the mesh. The Y stress is not constant in the mesh as expected. Figure 5.10 is a line plot of the X stress and shows that the stress is constant along the line. The Y stress is not constant along the line of Figure 5.9 because the solution is not completely converged due to a loose convergence tolerance. As the solver algorithm seeks a solution, the stresses reach local equilibrium with the fluid pressures. Global equilibrium of the blocks near the extraction well is not satisfied, and these blocks must translate to drive the boundaries of the reservoir out against the boundary springs. This will increase the loads in the boundary springs and result in global equilibrium. Figure 5.9 shows that the local stresses in the rock masses have come up to the current fluid solution, but the rock masses have not translated to bring the forces and stresses to equilibrium in the mesh. The Y displacement history plots in Figure 5.11 show this. Node 450 is in the bottom third of the finite element mesh and node 1950 is

in the top third of the mesh. Both nodes have increasing positive displacements, but from Figure 3.4, interface material three, we see that the displacements at the top of the mesh need to be more than twice the current displacement of node 1950 for the mesh to be in equilibrium.

Again, due to the extremely stiff joint model, the time step was reduced by a factor of 100. As a result, problem run times for complete convergence would be excessive. None the less, it appears that the local solution for the pressure is approximately correct, since local convergence has been obtained and the translations shown in Figure 5.10 are in the expected direction.

Two factors must be addressed to obtain a completely converged solution. First, we can speed the solution by using an effective joint law with the same flow characteristics but a softer effective structural stiffness (Chapter VI). Secondly, we must consider whether it is realistic to allow blocks to "float". For the conditions discussed in Section 5.2 the blocks should be held in place by shear forces applied by the X normal stress that is still acting on the blocks, even though a shear model is not implemented at this time. It may be more realistic to tie each block to ground to limit rigid body motion. Even if the injection pressure is above both in-situ stresses, one would not expect blocks as large as the ones in this model to be completely floating.

5.3 Transient Flow Problem

This problem uses the same finite element mesh as the two previous problems. The same joint opening law and boundary spring stiffnesses are also used. No far field fluid loss is allowed at the reservoir boundary. As mentioned before, this problem models a constant flow rate shut-in test which was a part of experiment #2070 conducted by LANL at Fenton Hill, New Mexico. Water was pumped into the HDR reservoir at a flow rate of 10.1e-3 m^3/s (133 gpm). The pressure was monitored at both the injection well and the shut-in extraction well. Figure 5.12 shows the measured pressure history at the injection well during experiment #2070.

This test is analogous to verification problem two, where a single joint was pumped up like a balloon, then allowed to collapse. For the current problem the shut-in extraction well pressure is monitored as the reservoir is being inflated. Because a single flow rate boundary condition will not yield a unique pressure solution, the pressure history monitored at the injection well during test #2070 was applied and the resulting input flow rate and shut-in extraction pressure were monitored. Figure 5.13 is a plot of the applied injection well pressure history and a plot showing the application point. For this problem the bottom of the mesh is considered a line of symmetry with no fluid flow through this boundary. This allows us to model a reservoir that is twice as large as could be modelled otherwise. Because solution times are basically linear with problem size, the run time was reduced by about half.

Figure 5.14 is a pressure contour plot for the first time step of the transient fluid solution. Recall that the injection well was located in the lower left corner of the mesh and that no flow is allowed out of the mesh. The pressure at the injection well did rise to the specified pressure and there is a significant pressure gradient from that point to the top of the mesh. The minimum pressure in the mesh is 0.97 MPa, only slightly above the initial pressure of 0.7 MPa.

Figure 5.15 is a plot comparing the measured output pressure history for well EE-2 (shut in pressure history) to the calculated pressure history from the transient boundary conditions discussed above. The far field flow loss was zero, so all the flow into the reservoir was accommodated by the joint openings. The results show that the calculated output pressure increases faster than the measured response.

This problem is an initial attempt to simulate a reservoir experiment. It demonstrates that the features needed to model the experiment are working, however, a careful review of input assumptions is needed to develop the final reservoir model. Three factors can easily slow the transient response of our model: increasing the reservoir volume, introducing a far field flow loss, and changing the time step size.

Increasing the number of flow paths will slow the transient response by producing additional fluid storage volume. Experimental data indicates that during hydrofracturing tests on the Phase II reservoir, 99% or more of the injected fluid volume was accommodated by aseismic tensile fracturing (Brown, 1988b). The present analysis corroborates this observation, with

nearly all input flow used to open tensile fractures. If more tensile joints are included in the model, then more fluid can be stored in the tensile joints, and it will take longer for the fluid to reach the shut in well. This will slow the shut-in transient.

Introducing a far field loss will slow the transient by producing leakage paths for the fluid. The far field flow loss is not well understood, but researchers at LANL (Brown, 1988a) feel that the far field flow loss for test #2070 was negligible (less than 2 % of the injection flow rate). In the present analysis, no far field loss was assumed.

Finally, changing the time step size may affect the response. If the time step in the solution is too large, the solution approaches the steady state solution. As the time step is reduced, the results converge to the transient solution. Additional calculations are needed in which we vary the time step size to examine convergence.

5.4 Summary

Three applications problems were presented in this chapter. The low pressure steady state problem showed that although good results can be obtained for a large problem, care must be taken to insure that the problem is converged. The high pressure steady state problem confirmed this. With the injection well pressure above the in-situ Y stress, the blocks were "floating" in the Y direction. Large translations in the mesh are required of most of the mesh to compress the boundary springs enough to balance the stress applied by the high fluid pressure. However, the fluid solution

should not be significantly affected by these translations because the mesh has come to a local equilibrium and because the rigid body translation does not affect the three major shear flow paths where the majority of the pressure drop occurs between the inlet an outlet wells. The transient problem displayed many of the same convergence characteristics as the high pressure steady state problem because of pressures above the Y in-situ stress. The transient results are encouraging, but the effects of the fluid time step, reservoir volume and far field flow losses need to be investigated. The solution run times for each of these problems was significantly slowed by the stiff interface elements.

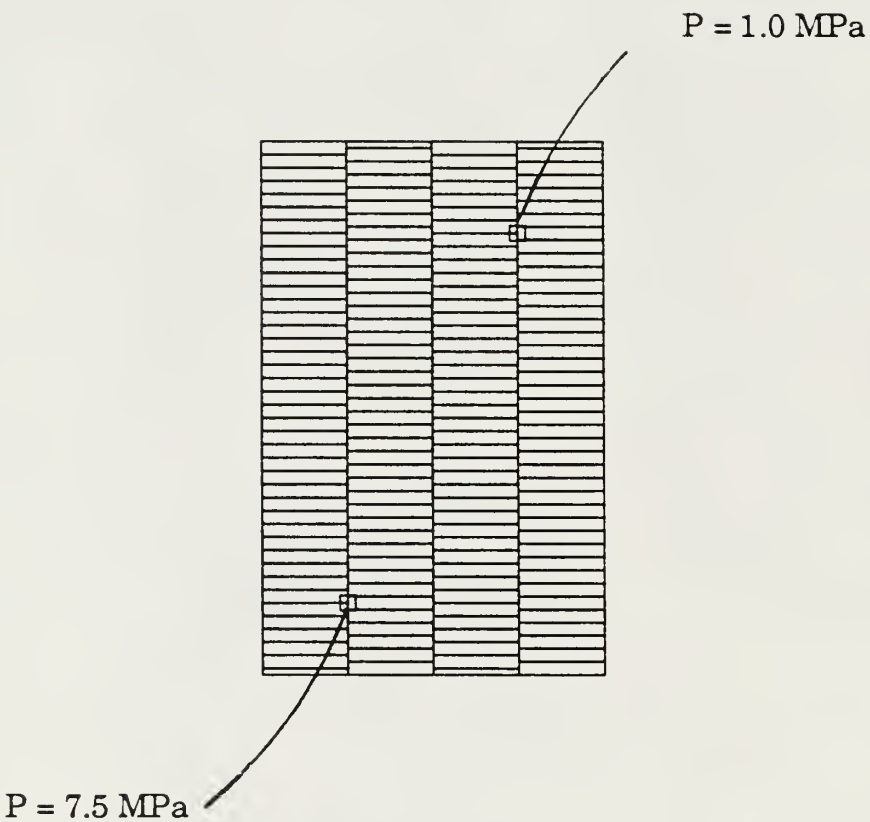

Figure 5.1: Boundary Conditions
(low pressure steady state problem)

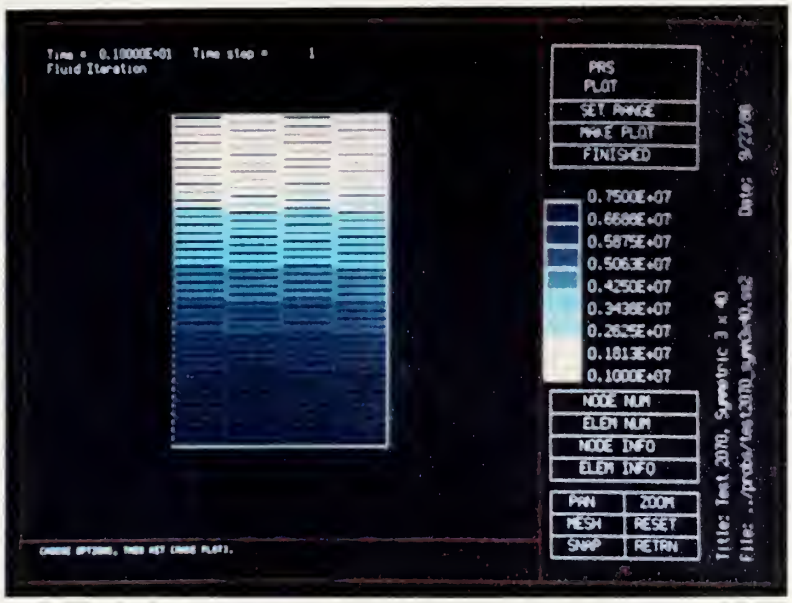

Figure 5.2: Pressure Contour Plot
(low pressure steady state problem)

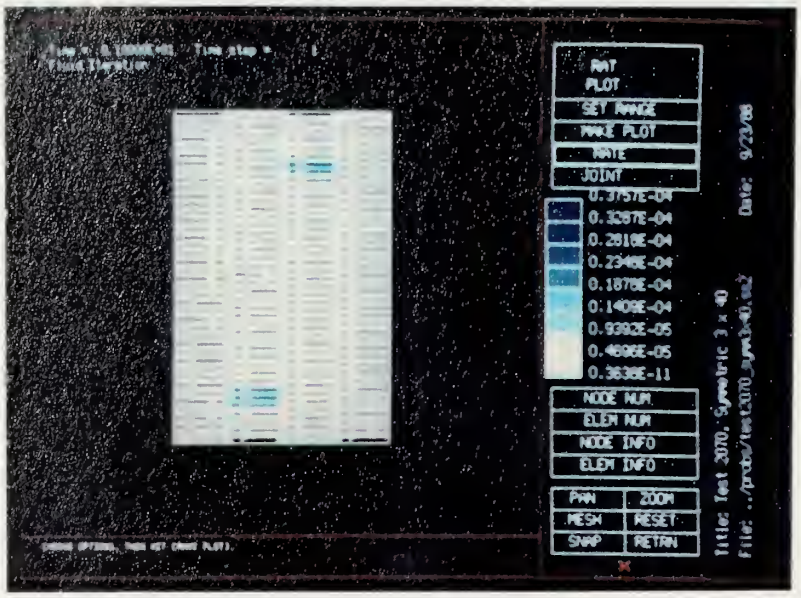

Figure 5.3: Flow Rate Contour Plot
(low pressure steady state problem)

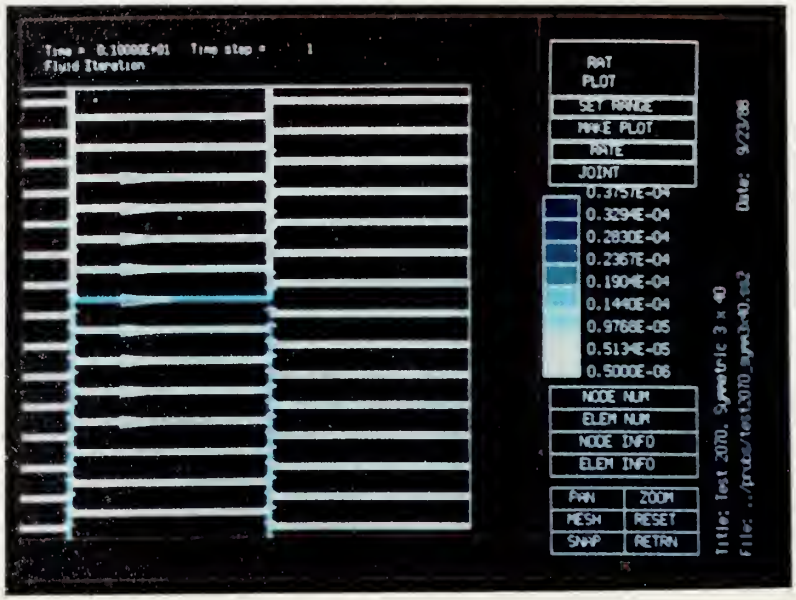

Figure 5.4: Flow Rate Contour, Zoom Around Extraction Well
(low pressure steady state problem)

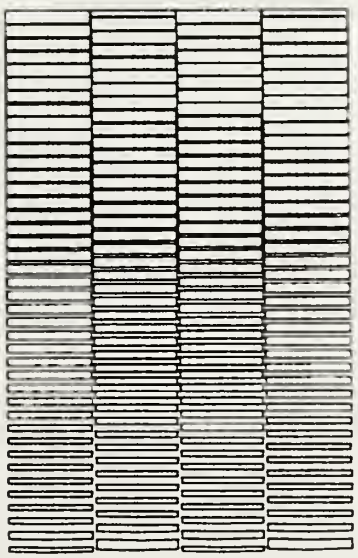

Figure 5.5: Displaced Mesh Plot
(low pressure steady state problem)

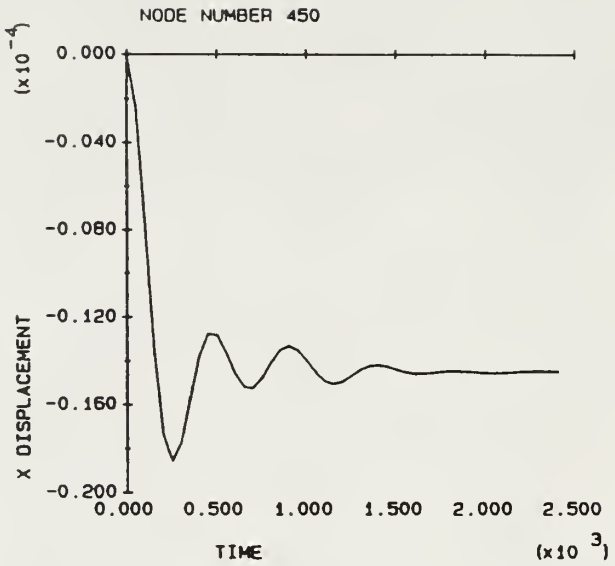

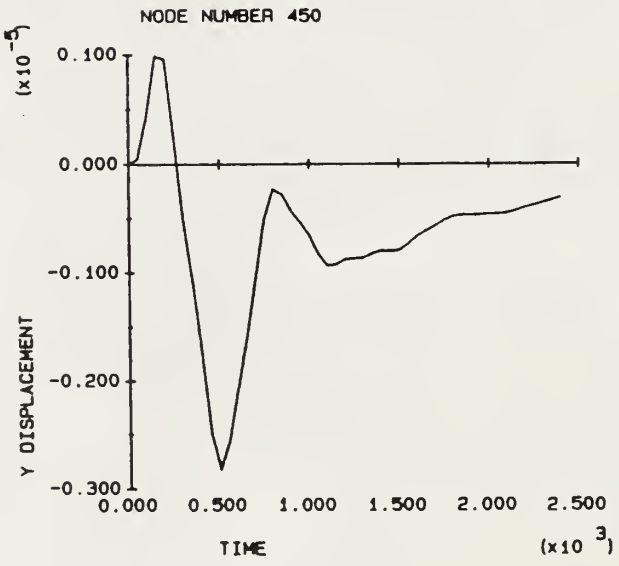

Figure 5.6: Displacement History Plots
(low pressure steady state problem)

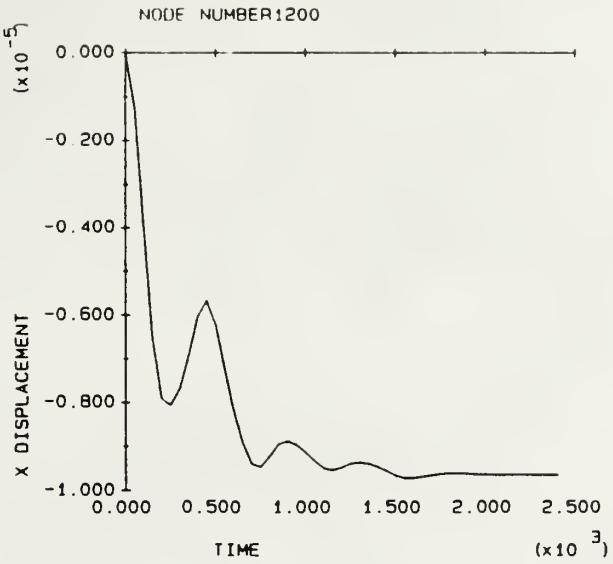

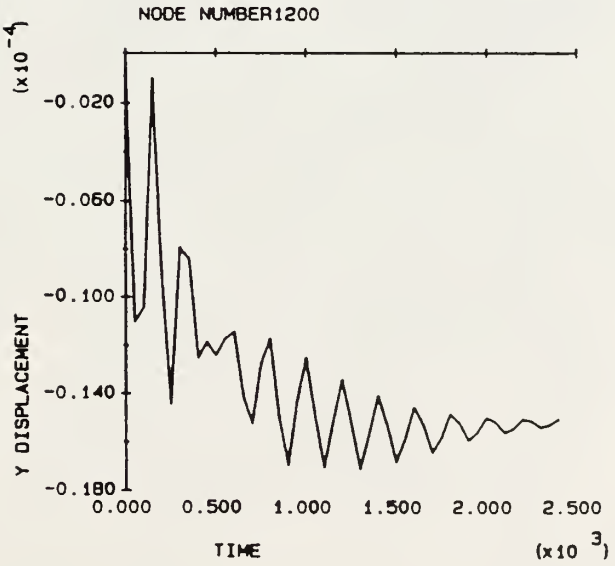

Figure 5.6 cont: Displacement History Plots
(low pressure steady state problem)

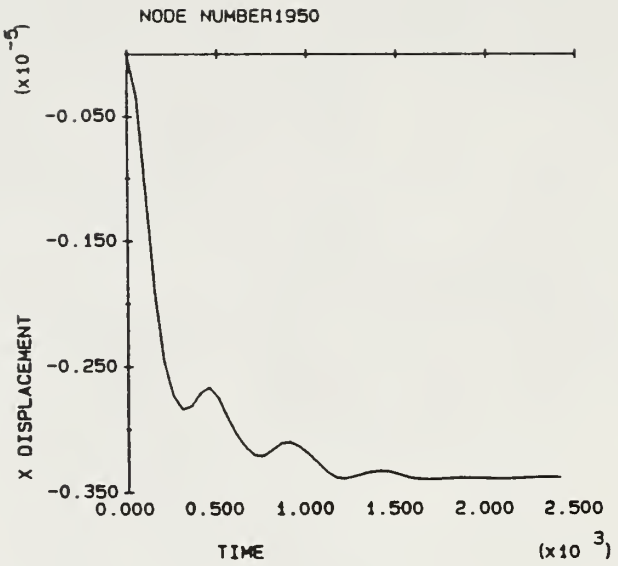

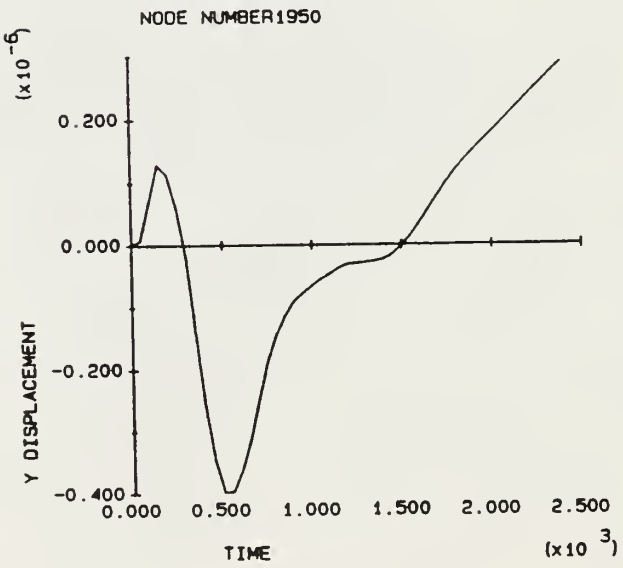

Figure 5.6 cont: Displacement History Plots
(low pressure steady state problem)

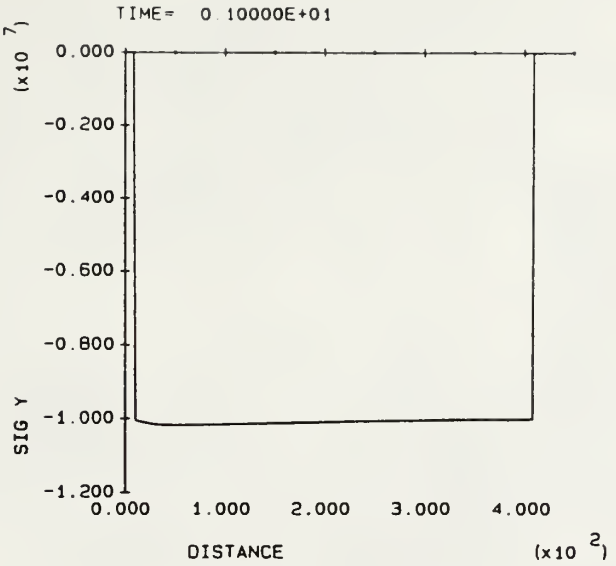

Figure 5.7a: Y Stress Line Plot
(low pressure steady state problem)

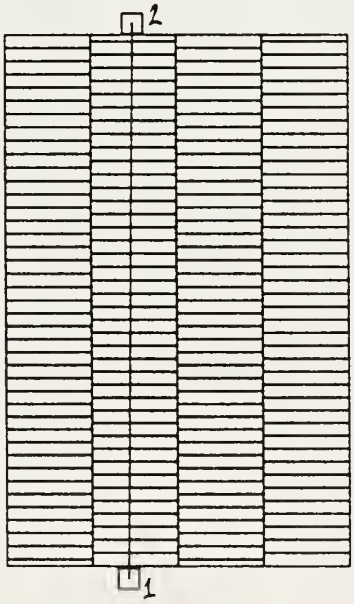

Figure 5.7b: Line of Application for Above Line Plot

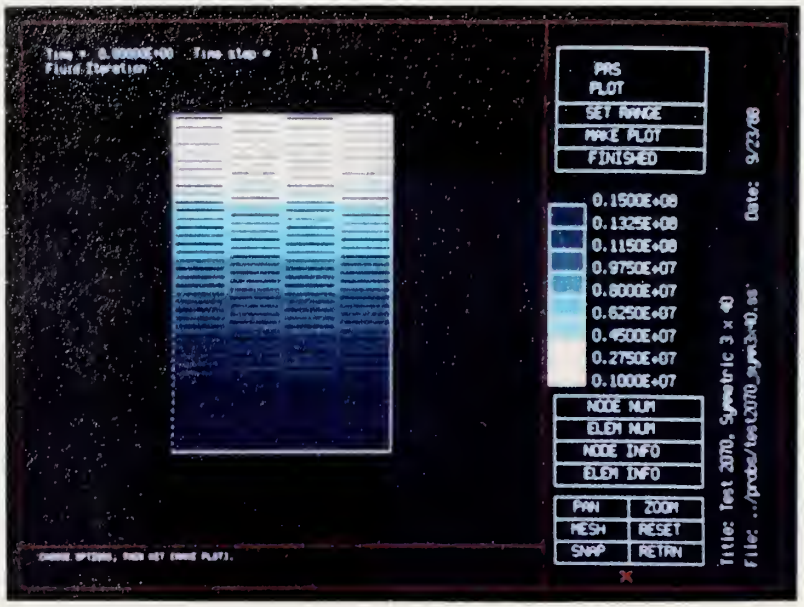

Figure 5.8: Pressure Contour Plot
(high pressure steady state problem)

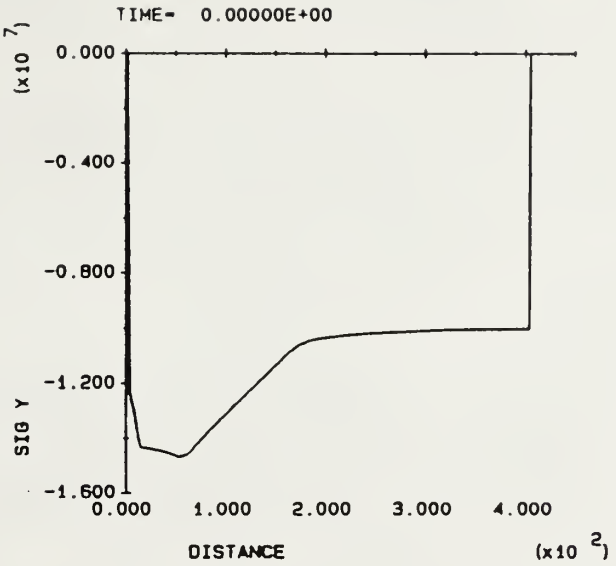

Figure 5.9a: Y Stress Line Plot
(high pressure steady state problem)

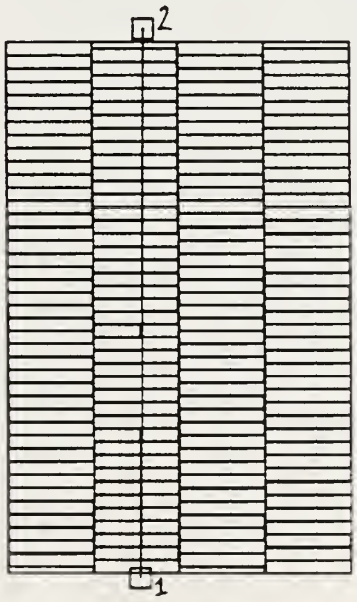

Figure 5.9b: Line of Application for Above Line Plot

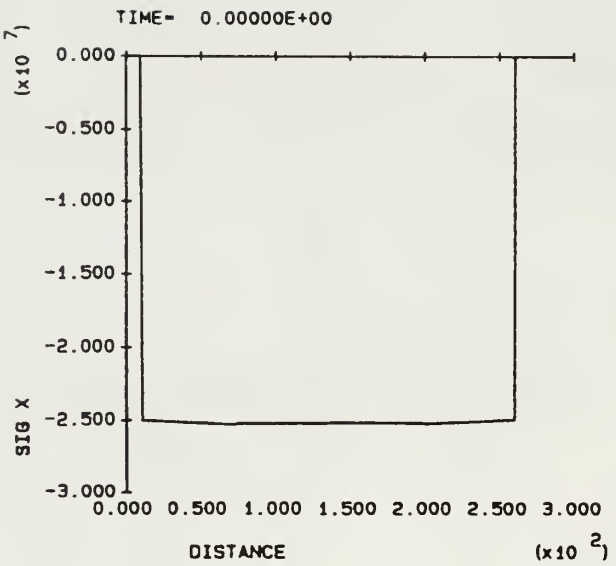

Figure 5.10: X Stress Line Plot
(high pressure steady state problem)

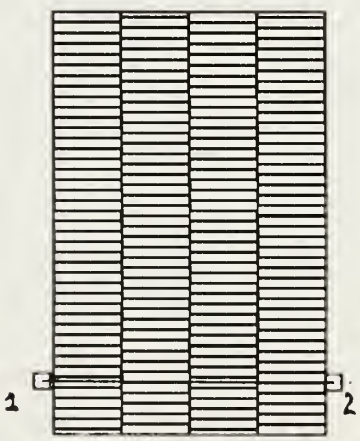

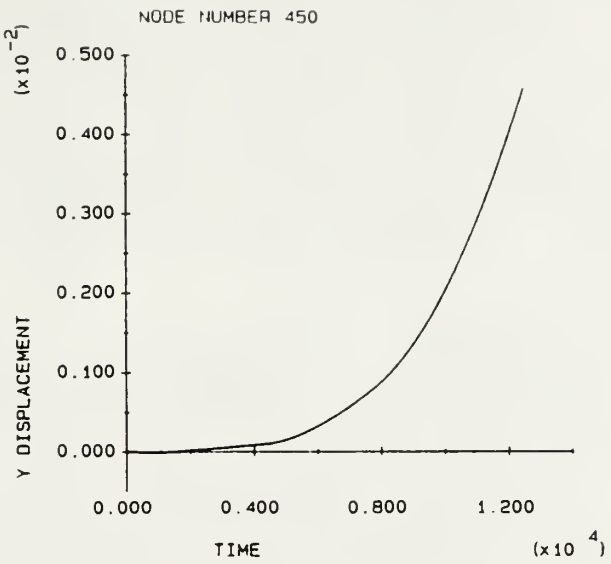

a) Bottom 1/3 of Mesh

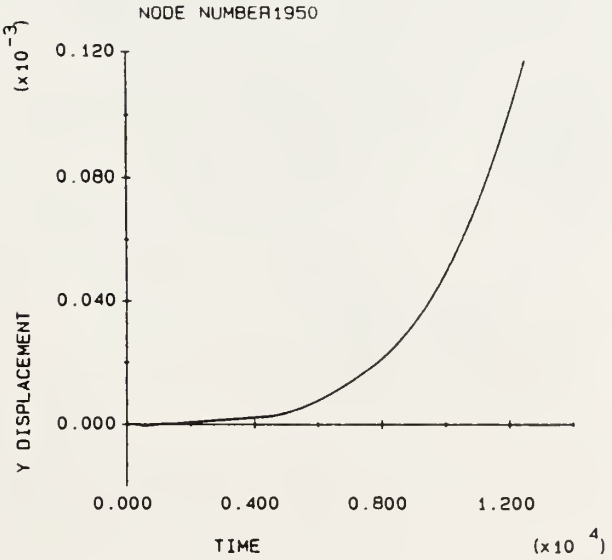

b) Top 1/3 of Mesh

Figure 5.11: Displacement History Plots
(high pressure steady state problem)

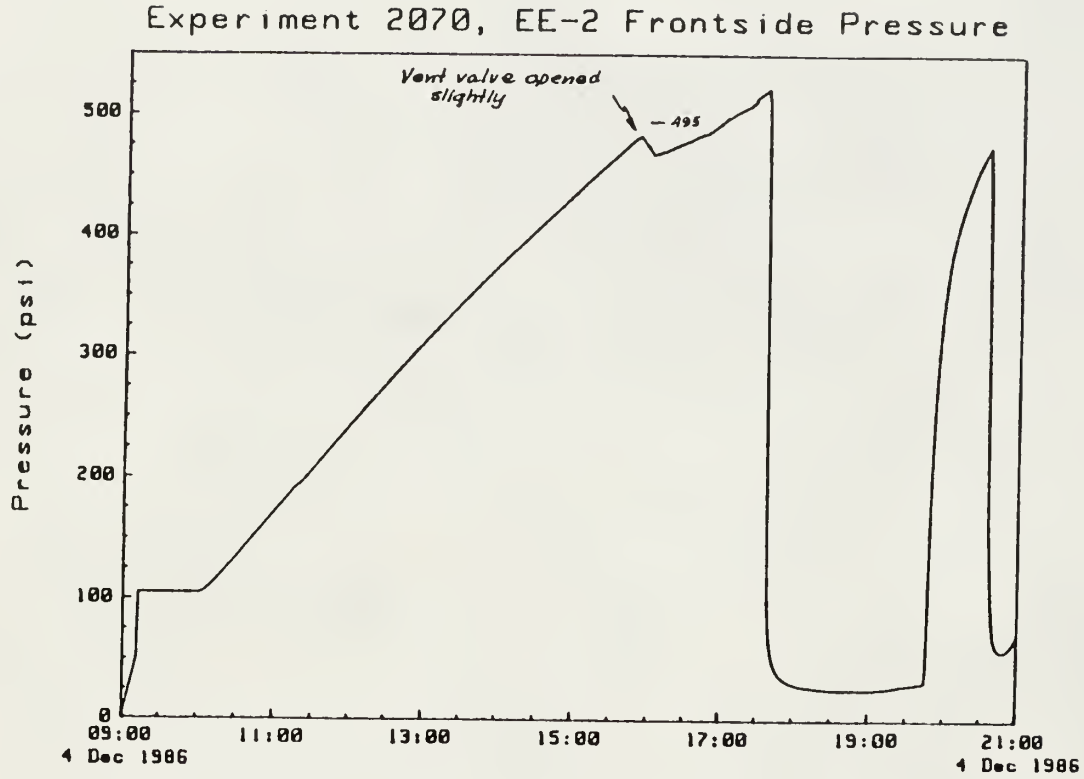

Figure 5.12: Experimental Extraction Well Pressure Results, Experiment #2070

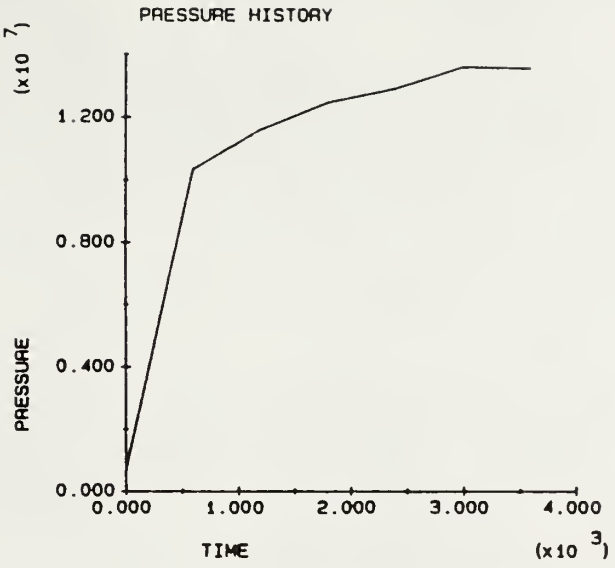

a) Pressure History

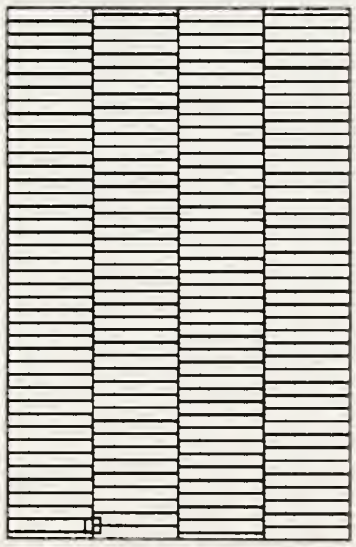

b) Application Point

Figure 5.13: Applied Pressure Boundary Condition (transient application problem)

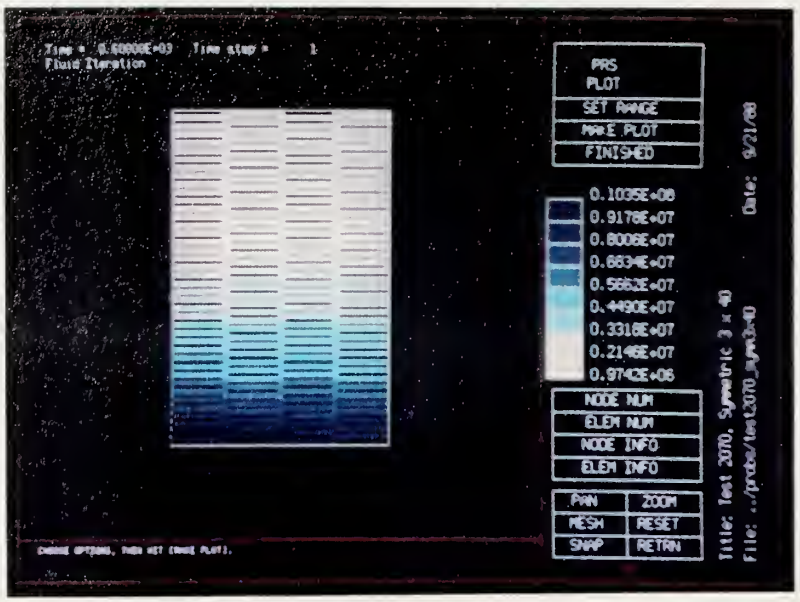

Figure 5.14: Pressure Contour Plot, First Transient Step (transient application problem)

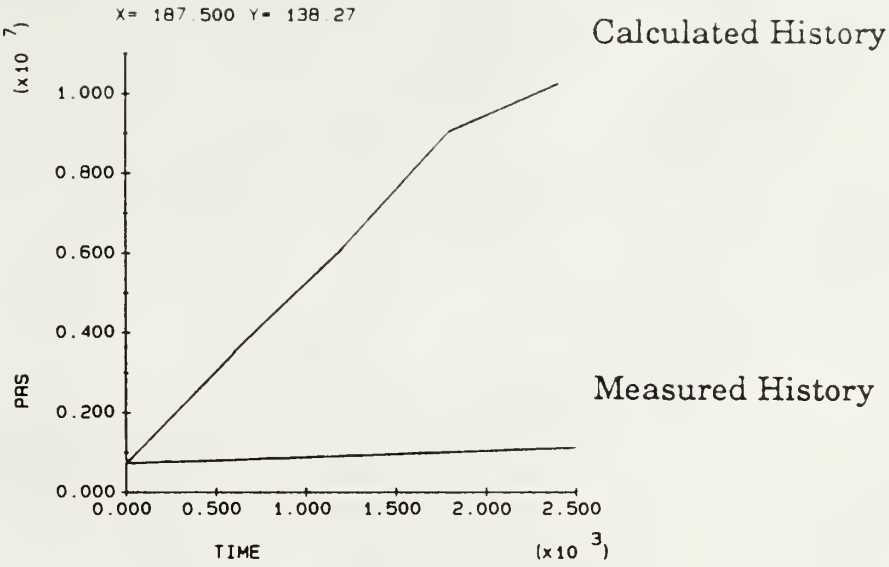

a) History Comparison One

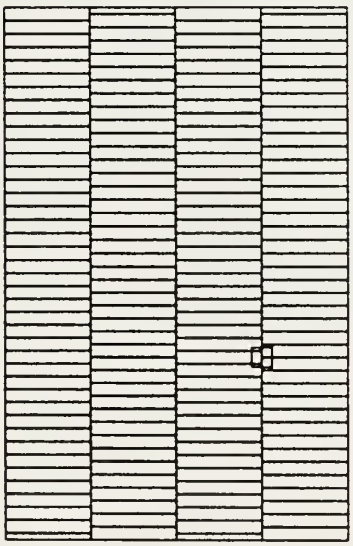

b) Calculation Monitor Point

Figure 5.15: Comparison of Calculated and Experimental Output Pressure Histories (transient application problem)

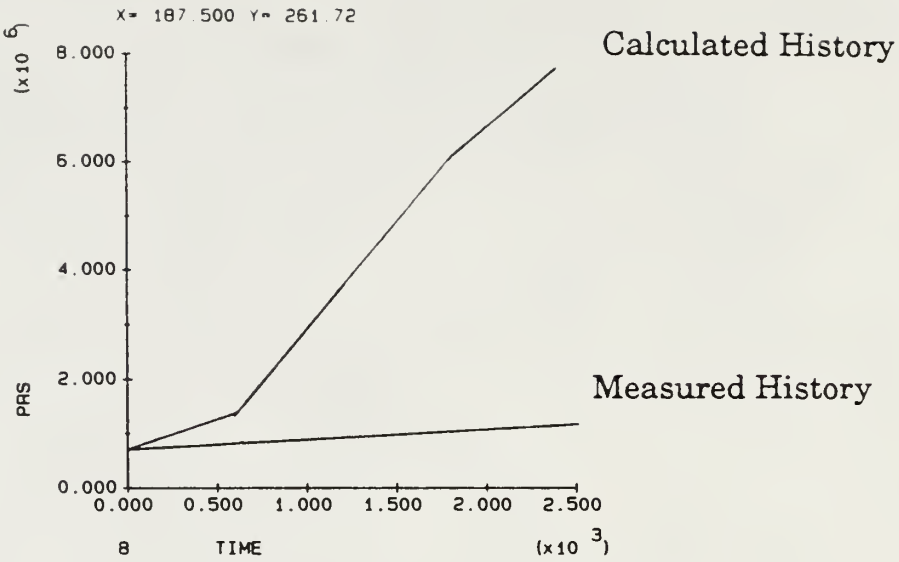

a) History Comparison Two

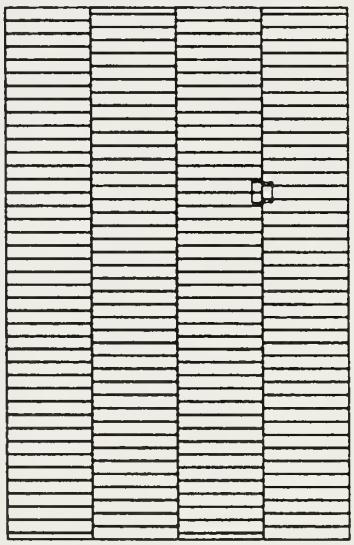

b) Calculation Monitor Point

Figure 5.15 cont: Comparison of Calculated and Experimental Output Pressure Histories (transient application problem)

Chapter VI

Summary and Conclusions

This chapter gives a summary of the thesis and explains the conclusions that can be drawn from the verification and application problems. Finally, recommendations are made for future work both for extending DRACULA's capabilities and for modelling HDR reservoirs with DRACULA.

6.1 Summary

In Chapter I we introduced the Hot Dry Rock concept. A brief history of the Hot Dry Rock program was presented to better understand the past modelling and experimental results.

In Chapter II the theoretical basis for the finite element method solution was developed for both the structural and fluid models. The structure is assumed linear elastic. A six noded quadratic triangle is used to approximate the structural solution. The fluid flow rate is assumed proportional to the pressure gradient and the joint permeability, which is a cubic function of the joint openings. A three noded quadratic line element is used to approximate the fluid solution. A surface element is presented which when superimposed on top of the fluid element models the joint opening law influenced by fluid pressures. The highly nonlinear nature of the problem was discussed and dynamic relaxation was presented as a solution method capable of solving the problem.

Chapter III presents the computer code DRACULA written to implement the concepts introduced in Chapter II. The interactive nature of DRACULA gives the user the ability to specify a problem and monitor the results all in the same interactive graphics environment. Next, some input data for DRACULA was discussed as it relates to the boundary conditions for the reservoir.

In Chapter IV we presented verification problems which illustrate that DRACULA can solve highly nonlinear steady state and transient fluid flow problems. We showed that flow rate and far field flow loss boundary conditions can be combined in one problem and also showed that the choice of the time step size for transient problems is important.

Three applications of DRACULA were illustrated in Chapter V. The first problem showed that good, converged results on these nonlinear problems are attainable even on large problems. Because all the fluid pressures were below the in-situ stress, the joint laws acted as expected with softer tensile joints opening more than the stiffer shear joints. Very little pressure drop was seen in the tensile joints compared to the shear joints.

The second and third problems both had fluid pressures above the minimum in-situ stress, but below the maximum in-situ stress. Convergence was reasonably good locally where fluid pressures were above the minimum in-situ stress, but rigid body translation of many of the blocks in the mesh are required before global convergence can be attained. Excessive run times are required for these problems because the joint

stiffnesses of the interface elements required the integration time step to be reduced by a factor of 100 to maintain stability. The third problem also showed that the fluid time step size, reservoir far field boundary conditions and number of fluid flow paths should be evaluated to obtain a model transient response that is closer to the experimental transient response.

6.2 Conclusions

An analysis tool was constructed that is useful for analyzing Hot Dry Rock reservoirs. However, a careful review of the initial and boundary conditions is needed to develop a final reservoir model.

Low pressure problems are easier to model than high pressure problems because for fluid pressures less than the in-situ stresses the joints do not open. Therefore the mesh is not required to translate large distances to bring the mesh to equilibrium.

High pressure problems (those with fluid pressures above the minimum in-situ stress) converge reasonably well at a local level, with local structural stresses rising to local fluid pressures, but the rigid body modes required to achieve global equilibrium need longer run times.

The transient problem was essentially a set of high pressure problems and displayed the characteristics discussed above. For the mesh and t-step used, the transient response was much too fast compared to the experimental data. The second verification problem showed that reducing t-step can improve a solution. The effects of t-step on this problem should be investigated.

The tensile joints have a strong effect on the flow. They have a larger initial opening (slightly) and they open up farther. They have higher flow rates with less pressure drop. For each problem investigated, the injection point was offset in the mesh to attempt to force flow across the mesh, but for each case the injection point location seemed to have little bearing on the results. The pressure horizontally across the bottom of the mesh was essentially constant and the flow rates in the shear paths from the injection well to the extraction well were constant and equal for each flow path.

Loose convergence tolerances on the structure gave adequate fluid results for the low pressure problem, but the fluid results for the high pressure problem may change slightly when the problem is truly converged. The pressures near the extraction well are fixed at 1.0 MPa. The joint stress must increase to about 14 MPa for a total stress of 15.0 MPa to balance the injection fluid pressure. Stresses this high in an interface element will require joint closure. This will be true for both the tensile and shear joints. These smaller displacements will definitely affect the flow solution, probably by causing higher pressure gradients near the extraction well.

The joint law is ≈100 times stiffer than the structural elements. This necessitates reducing the time step by a factor of 100 to insure numeric stability. If the spring stiffness could be reduced without affecting the fluid solution the time step reduction factor could be increased and solution times significantly reduced.

Even though the tolerance for a problem may be reasonable for a good solution for some problems, other problems may require tighter tolerances for good solutions. The results from the two steady state problems show this. The problem with the 7.5 MPa injection pressure converged to a reasonable solution with a structure tolerance of 0.1e-3 and a fluid tolerance of 0.5e-4. However, the 15 MPa injection pressure problem did not converge with the same tolerances and the same damping and coupling parameters. This problem required tighter tolerances and less damping for better convergence.

6.3 Recommendations

As discussed in Section 3.1 the solution algorithm is significantly slowed by the extremely stiff joint opening law. One method of removing this constraint is to artificially soften the joint stiffness for the global structural solution, but still recover the joint openings using the original joint opening law. This could be implemented by putting a relatively soft spring in series with the joint law for the structural solution. This would not significantly affect the structural solution. If this method were to work the solution time could be reduced by a factor of 100.

The results of the transient problem in Section 5.3 are encouraging from the stand point that transient results were obtained for such a large highly nonlinear problem, but the results did not match well with the experimental results from test #2070 conducted by LANL. Three major factors can affect the transient results of these transient problems: (1) the fluid time step size, (2) the reservoir volume and the distribution of volume

between shear and tensile fractures, and (3) far field fluid boundary conditions. Each of these should be studied to better understand their effects on transient problems.

The results of this thesis are a foundation on which to build a fully coupled heat transfer, fluid flow, rock deformation analysis code. The fluid flow and rock deformation models are now fully coupled. The next step is to include temperature dependent fluid viscosity, thermal stresses and a heat transfer model for heat flow between the structure and the fluid.

Dynamic relaxation has proven to be a very reliable solution method for these nonlinear problems. In addition it has the virtue of approximately linear solution time increase with problem size. However, it is not a fast solution method. Many other methods exist that are reasonably robust with good initial guesses on the solution and are much faster than dynamic relaxation. Since dynamic relaxation seems to be at its worst when it is near a solution, other methods should be investigated with the intent that dynamic relaxation would start the problem and an alternate solution used for final convergence. The effects of the rigid body modes of many of the blocks in the finite element mesh must be considered when investigating a new solution algorithm.

Some of the "floating" block problems described in Section 5.3 would not present themselves if a shear law existed in the model. If a shear model is implemented, DRACULA should be modified such that the joint laws are entered in terms of the principal stress orientation rather than as data in a table. This would allow the effects of the principal stress

orientation to be investigated much more easily than with the current joint law implementation.

References

Armstead, H. Christopher H., 1978, *Geothermal Energy*, E. & F.N. Spon, Ltd, pp. 203 - 213.

Asgian, M.I., 1988a, "A numerical study of Fluid Flow in Deformable, Naturally Fractured Rock Masses," Submitted to *Int. J. Rock Mech. Mining Sci. & Geomech. Abstr.*

Asgian, M.I., 1988b, "A numerical study of fluid flow in a deformable, naturally fractured reservoir: The influence of pumping rate on reservoir response," *Key Questions in Rock Mechanics: Proceedings of the 29th U.S. Symposium.*

Birdsell, Steven A. and Robinson, B.A., 1988, "A Three-Dimensional Model of Fluid , Heat, and Tracer Transport in the Fenton Hill Hot Dry Rock Reservoir", Presented at the Thirteenth Annual Workshop on Geothermal Reservoir Engineering, Stanford University, CA, Jan. 19-21.

Brown, Donald W., 1988a, Los Alamos National Laboratory, ESS-4, Personal Communication.

Brown, Donald W., 1988b, "Anomalous Earth Stress Measurements During a Six-year Sequence of Pumping tests at Fenton Hill, New Mexico," *Proceedings of the Second International Workshops on Hydraulic Fracturing Stress Measurements*, June 15-18, Vol. 1, pp 451-475.

Brown, Stephen R., 1987, "Fluid Flow Through Rock Joints: The effect of Surface Roughness," *Journal of Geophysical Research*, Vol 92, No. B2, pp 1337-1347.

Cundall, Peter A., 1982, "Fluid-Rock Interaction Program (FRIP) Manual," Internal report - University of Minnesota, Dept. of Civil and Mineral Engineering.

Duncan, Neil, 1969, *Engineering Geology and Rock Mechanics*, International Textbook Co. Ltd., London, England.

Franke, Paul R., 1988, "The U.S. Hot Dry Rock Geothermal Energy Development Program", Presented at Geothermal Resources Council Geothermal Energy Symposium, New Orleans, Jan. 10-14.

Gangi, Anthony F., 1978, "Variation of whole and Fractured Porous Rock Permeability with confining Pressure," *Int. J. Rock Mech. Min. Sci. & Geomech Abstr.*, Vol 15, pp 249-257.

Hilber, Hans M. and Robert L. Taylor, 1976, "A Finite Element Model of Fluid Flow in Systems of Deformable Fractured Rock," Department of Civil Engineering, Division of Structural Engineering and Structural Mechanics, University of California, Berkeley, CA.

Kelkar, Sharad, Zora Dash, Mark Malzahn, and Robert Hendron, 1987, "Hydraulic and Thermal behavior of a Hot Dry Rock Reservoir during a 30-day Circulation Test," Presented at Geothermal Resource Council 1987 Annual Meeting, Sparks, NV, October 11-14.

Los Alamos National Laboratory Hot Dry Rock Geothermal Energy Development Program, 1979, Fiscal Year Annual Report LA-8280-HDR.

Los Alamos National Laboratory Hot Dry Rock Geothermal Energy Development Program, 1981, Fiscal Year Annual Report LA-8287-HDR.

Noorishad, J., M.S. Ayatollahi, and P.A. Witherspoon, 1982, "A Finite Element Method for Coupled Stress and Fluid Flow Analysis in Fractured Rock Masses," *Int J. Rock Mech. Min. Sci. & Geomech. Abstr.*, Vol 19, pp 185-193.

Pine, R.J.and A.S. Batchelor, 1984, "Downward Migration of Shearing n Jointed Rock During Hydraulic Injections," *Int. J. Rock Mech. Min. Sci. & Geomech. Abst.*, Vol. 21, No. 5, pp 249-263.

Pine, R.J., P.A. Cundall, 1985, "Applications of the Fluid Rock Interaction Program (FRIP) to the Modelling of Hot Dry Rock Geothermal Energy Systems," *Proceedings of the International Symposium on Fundamentals of Rock Joints*, Bjorkliden, Sweden, September 15-20.

Pine, Robert J.and Peter Ledingham, 1984, "In-Situ Hydraulic Parameters for the Carnmenellis Granite Hot Dry Rock Geothermal Energy Research Reservoir," *Journal of Petroleum Technology*, November, pp 1982-1990.

Robinson, Bruce A., 1985, "Non-Reactive and Chemically Reactive Tracers: Theory and Applications," Ph.D. Thesis, MIT, February, 1985.

Robinson, Bruce A., 1988, "Fracture Network Modeling of A Hot Dry Rock Geothermal Reservoir," Presented at the Thirteenth Annual Workshop on Geothermal Reservoir Engineering, Stanford University, Stanford CA, January 19-21.

Ryan, Thomas M. and Ian W. Farmer, 1987, "Laboratory determination of Fracture Permeability," *28th U.S. Symposium on Rock Mechanics*, Tucson, AZ.

Snow, D.T., 1965, "A Parallel Plate Model of Fractured Permeable Media," Ph.D. thesis, University of California, Berkeley.

Su, Shun-Lung, 1988, "A Finite Element Method Solution for Fluid Flow in Jointed Rock," M.S. Thesis, Kansas State University, Manhattan, KS.

Swenson, Daniel V., 1985, "Modeling Mixed-Mode Dynamic Crack Propagation using Finite Elements," Ph.D. thesis, Cornell University, Ithaca, NY.

Underwood, Philip, 1983, "Computational Methods for Transient Analysis," Elsevier, Science Publishers B.N., pp. 245 - 265.

Whetten, J.T., H.D. Murphy, R.J. Hanold, C.W. Meyers, and J.C. Dunn, 1988, "Advanced Geothermal Technologies", Presented at Energy technology Conference & Exposition, Washington DC, Feb. 17-19.

Witherspoon, P.A., J.S.T. Wang, K. Iwai, and J.E. Gale, 1980, "Validity of the cubic law for fluid flow in a deformable rock fracture," *Water Resources Research*, Vol. 16, No. 6.

Zienkiewicz, O.C., 1977, *The Finite Element Method*, McGraw Hill, Third Edition, pp 196-201.

Zyvolosky, G., Z.V. Dash, and S. Kelkar, 1988, "FEHM: Finite Element Heat and Mass Transfer Code," Los Alamos National Laboratory Manuscript, Report LA-11224-MS.

A FINITE ELEMENT MODEL OF FLUID FLOW IN JOINTED ROCK

BY

MARK A. JAMES

B.S., Kansas State University, 1986

AN ABSTRACT OF A MASTER'S THESIS

submitted in partial fulfillment of the

requirements for the degree

MASTER OF SCIENCE

Department of Mechanical Engineering

KANSAS STATE UNIVERSITY
Manhattan, Kansas

1988

ABSTRACT

Hot Dry Rock geothermal reservoirs are currently being developed around the world. Extensive experimental work has been done, but few numerical models exist. This model solves the coupled fluid flow -- rock deformation problem and provides the foundation for fully coupled heat transfer with thermal stresses.

A computer program called DRACULA (Dry Rock Analysis Code) is used to model steady state and transient fluid flow results. The model uses discrete joints to model the fluid flow through the fractured rock. Two separate models are used in the program: (1) a structural model to solve for rock deformations, and (2) a fluid model to solve for fluid pressures. The two models are coupled through the joint permeability (cubic law) and the effective stress law. Dynamic relaxation is used to obtain solutions.

The formulation includes the transient storage terms associated with joint opening velocities. This allows the user to simulate reservoir operation in an inflation/deflation mode where fluid is pumped into the reservoir, stored by opening rock joints, and then recovered when the pressure is lowered.

Verification problems demonstrate that the fluid and structural models are correctly coupled. The first verification problem shows flow through a single flow path where joint opening is not uniform. The second illustrates inflation/deflation in a single flow path.

Results are presented for a more complex model simulation of the Fenton Hill reservoir. Results for flow between two wells at specified pressures show that the tensile joints (normal to the smallest in-situ stress) open and have higher flow rates with less pressure drop than the shear joints (normal to the maximum in-situ stress). When the injection pressure is raised above the minimum in-situ stress, the tensile joints completely open and rock masses "float". An initial simulation of a shut-in experiment at Fenton Hill demonstrates the storage effect of joint openings.

Recommendations are made on speeding solutions and further calculations needed to model the Fenton Hill reservoir.